

Research Paper

Tracking $\delta^{13}\text{C}$ and $\delta^{18}\text{O}$ fluctuations uncovers stable modes and key patterns of paleoclimateShifeng Sun ^a, Haiying Wang ^{a,*}, Yongjian Huang ^{b,c}^a School of Science, China University of Geosciences(Beijing), Beijing 100083, China^b State Key Laboratory of Biogeology and Environmental Geology, China University of Geosciences (Beijing), Beijing 100083, China^c School of Earth Sciences and Resources, China University of Geosciences(Beijing), Beijing 100083, China

ARTICLE INFO

Article history:

Received 20 September 2023

Revised 30 November 2023

Accepted 3 February 2024

Available online 10 February 2024

Handling Editor: Yirang Jang

Keywords:

Cenozoic climate dynamics
Correlation analysis
Complex network
Coarse-grained methods
Phase space reconstruction

ABSTRACT

The examination of fluctuations in the correlations between $\delta^{13}\text{C}$ and $\delta^{18}\text{O}$ is of significant importance for the reconstruction of the Earth's climate history. A key challenge in paleoclimatology is finding a suitable method to represent the correlated fluctuation system between $\delta^{13}\text{C}$ and $\delta^{18}\text{O}$. The method must be able to handle data sets with missing or inaccurate values, while still retaining the full range of dynamic information about the system. The non-linear and complex correlations between $\delta^{13}\text{C}$ and $\delta^{18}\text{O}$ poses a challenge in developing reliable and interpretable approaches. The transition network, which involves embedding the $\delta^{13}\text{C}$ and $\delta^{18}\text{O}$ sequence into the network using phase space reconstruction, is a coarse-grained based approach. This approach is well-suited to nonlinear, complex dynamic systems, and is particularly adept at emerging knowledge from low-quality datasets. We have effectively represented the fluctuations in the correlation between $\delta^{13}\text{C}$ and $\delta^{18}\text{O}$ since 66 million years ago (Ma) using a system of complex network. This system, which has topological dynamical structures, is able to uncover the stable modes and key patterns in Cenozoic climate dynamics. Our findings could help to improve climate models and predictions of future climate change.

© 2024 China University of Geosciences (Beijing) and Peking University. Published by Elsevier B.V. on behalf of China University of Geosciences (Beijing). This is an open access article under the CC BY-NC-ND license (<http://creativecommons.org/licenses/by-nc-nd/4.0/>).

1. Introduction

The $\delta^{13}\text{C}$ and $\delta^{18}\text{O}$ records are the most widely used tools for reconstructing Earth's climate history (Westerhold et al., 2020), and their complex relationships are critical for understanding the dynamics of the Cenozoic climate system. However, the underlying mechanisms governing these intricate relationships remain multi-faceted, involving complex interactions between biomes, astronomical forcing, ice sheet changes, fresh water fluxes, and burial of organic matter in the ocean (e.g. Bouttes et al., 2012; Turner, 2014; De Vleeschouwer et al., 2020; Ma et al., 2022; Cornault et al., 2023). These complex relationships arise not only from the direct causal effects of these mechanisms but also from autocorrelation effects, indirect links, or common drivers embedded within the $\delta^{13}\text{C}$ and $\delta^{18}\text{O}$ sequences (Runge et al., 2019; Nowack et al., 2020). To effectively capture these relationships of the $\delta^{13}\text{C}$ and $\delta^{18}\text{O}$ records and advance our understanding of Earth's climate history, we need methods that can accurately represent these

relationships. Such methods should be applicable to datasets with noise and missing values, and should not only ensure that important information is not lost, but also reveal the internal mechanisms of paleoclimate dynamics.

It is difficult to find an appropriate representation of correlated fluctuation system in the complex relationships between $\delta^{13}\text{C}$ and $\delta^{18}\text{O}$ data. This prevents accurate solutions of the relationships between two variables from long-term data. Causal inference is a powerful tool for analyzing geoscience data, providing deeper insight into the complex interactions between different phenomena. However, it can only address the relationships between variables within the framework of causal inference, and observational error and missing values can degrade causal inference (Runge et al., 2019). Traditional correlation analysis is crude and prone to subjective interference. Phase analysis can accurately analyze the relationships between two variables, but is sensitive to noise (Weng et al., 2018). Evolutionary spectral analysis focuses on how the frequency of the correlated signal changes over time. By focusing on frequency, evolutionary spectral methods can provide useful information. They can reveal the contributions of different components of the signal to the overall behavior. However, the evolutionary spectrum analysis is better suited to signals with

* Corresponding author.

E-mail address: whyct@126.com (H. Wang).

clear periodic features. It is difficult to deal with the signals of complex correlation fluctuations in paleoclimatology (Xiang et al., 2018). Wavelet analysis is commonly used to explore paleoclimate data. It can capture the non-stationarity and time-scale dependence of correlation sequences. However, this method requires careful parameter selection, as different parameters will affect the results. Furthermore, the interpretation of wavelet analysis results can be complex and subjective (Cauvy-Fraunié et al., 2013; Tomás et al., 2016; Gallegati, 2018).

Complex networks, also known as networks or graphs, are a common data structure that can be used to describe complex systems with correlated fluctuation of time series. Transition networks are a type of network using phase space reconstruction, tracing the succession of dynamical states over time. They are particularly suitable for missing and noisy data (Zhang et al., 2017; Zou et al., 2019). We refer to such correlation systems formed by embedding two time series in a network as correlated fluctuation system. This approach allows us to track how the correlation between $\delta^{13}\text{C}$ and $\delta^{18}\text{O}$ series in paleoclimate changes over time.

Inspired by recent advances in the analysis of nonlinear time series using complex networks (Myers et al., 2023), we present a novel coarse-grained based approach using phase space reconstruction to embed bivariate time series into a complex network. In particular, this coarse-grained based transition network proves adept at constructing correlation system from low-quality, long-term time series pairs. It demonstrates an impressive ability to robustly and reliably emerge knowledge about the underlying system dynamics (Morita, 2023). Experiments on the $\delta^{13}\text{C}$ and $\delta^{18}\text{O}$ records of deep-sea isotopes show that the method is effective in inferring stable modes and key patterns of correlated fluctuation systems, over an extensive 66 million-year timeframe. Given the complex and dynamically evolving interplay between $\delta^{13}\text{C}$ and $\delta^{18}\text{O}$ within the Earth system (Turner, 2014; Jolivet and Boulvais, 2021), this paper presents a novel and promising method for resolving the dynamical representation of the correlated fluctuation system. The capabilities demonstrated by this approach show a new and promising perspective for understanding the Cenozoic climate system.

2. Methods

2.1. To embed the correlation coefficients series on networks

The coarse-grained based transition networks are a powerful tool for studying the underlying dynamics of complex systems. The construction of such complex networks relies on a proper partitioning of the phase space, which can be achieved using the methods of phase space reconstruction (Zou et al., 2019). These methods use the concept of nonlinear dynamics to study the underlying dynamical information in time series data (Marwan et al., 2007; Boers et al., 2021). In this section, we first reconstruct the phase space of a correlated fluctuation system by mapping the two time series into the correlation series. And then the correlation series are mapped into a space of pattern vectors.

2.1.1. To find the correlation coefficients series

The correlation fluctuations of series with different time periods are measured using the time window method (Fig. 1A). We divide a pair of time series into some short segments of size l , called the time windows of size l . By computing the correlation coefficient of each segment, we observe the correlation fluctuations of the bivariate time series.

Let $T = \{(X_i, Y_i) | i = 1, \dots, m\}$ be a pair of time series of length m . Let (X_{t_1}, Y_{t_1}) and (X_{t_2}, Y_{t_2}) be the start and end points of the time

window, respectively. In a time window, the position of the center is $(t_2 - t_1)/2$ and the size is $l = t_2 - t_1$.

A correlation series $R = \{r_1, r_2, \dots, r_{m-l+1}\}$ is computed by sliding the time window over the entire time series T and computing the correlation coefficient over each time window. The length of the correlation series is $m - l + 1$. The setting of the time window can increase the stability of the system and adjust the resolution of the time series. A smaller time window size l results in a lower resolution of the correlation series, making the system less robust to missing data and outliers. However, a larger time window size l results in more overlapping time series segments, making the system more redundant and obscuring some important dynamic mechanisms. The power of the results depends on the size of the time window. All information within the time window is closely related to each specific correlation coefficient.

The correlation relationships between the two variables can be measured using Pearson's correlation coefficients, and the Pearson's estimator r_k is defined as,

$$r_k = \frac{\sum_{i=1}^m (X_i - \bar{X})(Y_i - \bar{Y})}{\sqrt{\sum_{i=1}^m (X_i - \bar{X})^2 \sum_{i=1}^m (Y_i - \bar{Y})^2}} \quad (1)$$

where $\bar{X} = \sum_{i=1}^m X_i/m$ is the sample mean of the variable X and $\bar{Y} = \sum_{i=1}^m Y_i/m$ is the sample mean of the variable Y , k is the index of the estimator r_k .

From Eq. (1), there exists a function $f : T \rightarrow R$ which maps a pair of time series into a correlation coefficients series.

To illustrate this process, we can consider an actual observed pair of time series. As shown in Fig. 1B, each time window of size l is computed by the correlation measure Eq. (1) as an estimate r_k representing its correlation. A set of such estimates forms the correlation coefficients series $R = \{r_1, r_2, \dots, r_{m-l+1}\}$ by

$$\begin{cases} r_1 = f[(x_1, y_1), (x_{1+\tau}, y_{1+\tau}), \dots, (x_{1+(l-1)\tau}, y_{1+(l-1)\tau})] \\ r_2 = f[(x_2, y_2), (x_{2+\tau}, y_{2+\tau}), \dots, (x_{2+(l-1)\tau}, y_{2+(l-1)\tau})] \\ \dots \\ r_{m-(l+1)\tau} = f[(x_{m-(l+1)\tau}, y_{m-(l+1)\tau}), \dots, (x_m, y_m)] \end{cases} \quad (2)$$

where l is the size of a time window and τ is the spacing of a time series sampling point used to control phase space partitioning. In this analysis of a correlated fluctuation system, we can choose $\tau=1$. This choice implies the selection of a successive sequence.

Such a phase space partition above maps the time series into the correlation series and preserves the correlation information of the series.

2.1.2. To reconstruct the space of pattern vectors

In the previous subsection, we obtained the series of the correlation coefficients. Then, a coarse-grained approach is used to reconstruct the representation space of the correlated fluctuation system. The coarse-grained approach refers to the process of simplifying complex systems by grouping their components into larger units. This process is often used in physics to make calculations more manageable or to reveal certain physical properties of specific system (Morita, 2023).

In our work, we adopt a coarse-grained approach to transform a correlation series into the correlated fluctuation system. This approach is based on the process of time series embedding using the coarse-grained transition network, which preserves the topological properties of the underlying dynamical system (Wang and Tian, 2016). This makes it easier to mine the underlying dynamic structure.

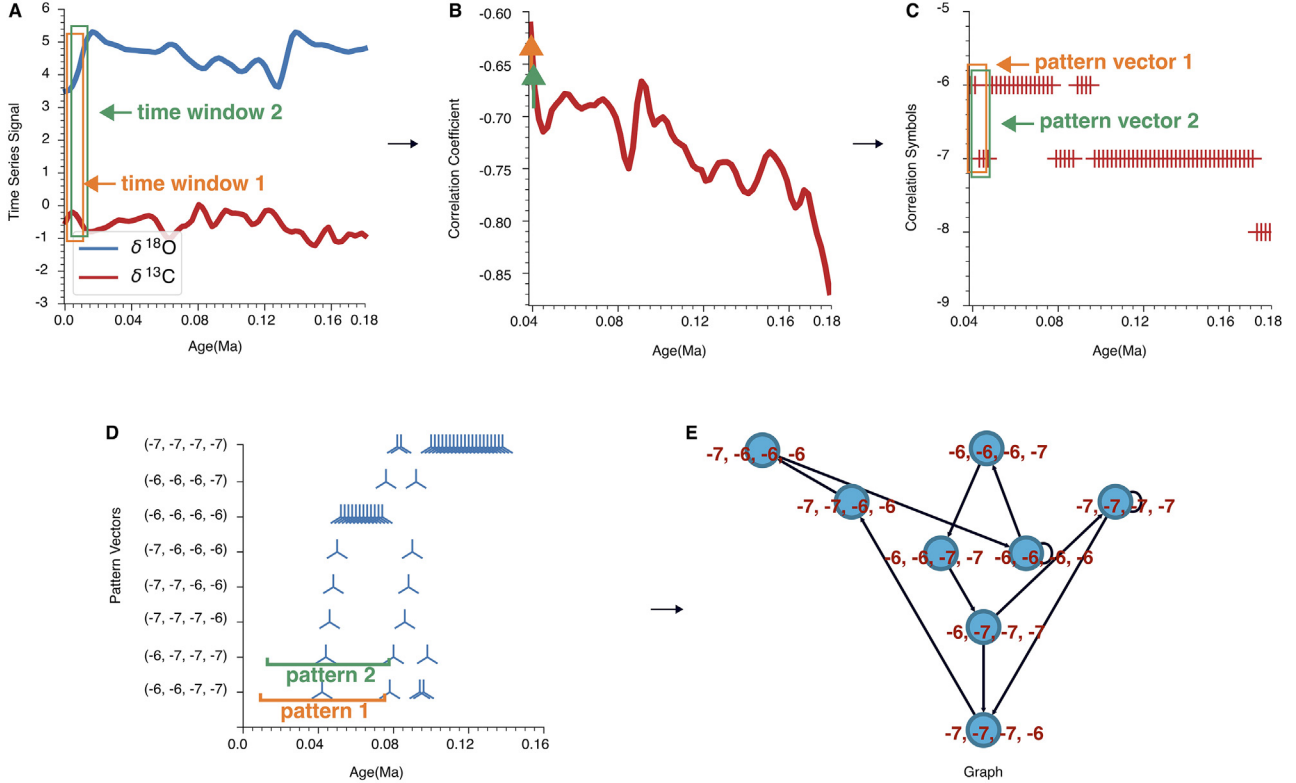


Fig. 1. The process of constructing a complex network from original data. In (A) we have extracted relevant information from the original data signals. The processes of coarsening the series of correlations into symbols are shown in (B) and (C). The steps from the reconstruction of the original data to the pattern vector space are shown in (A), (B), (C) and (D), where the midpoint of patterns duration is marked in (D). (E) shows the final complex network embedding of the correlation series.

Let A represent the correlation states of a correlated fluctuation system, and $\{s_1, s_2, \dots, s_p\}$ denote a set of p mutually disjoint correlation fluctuation states. Then $A = \{s_1, s_2, \dots, s_p\}$. To obtain equidistant selections, we let $p = 19$, and define $s_1 = 9, s_2 = 8, \dots, s_{10} = 0, s_{11} = -1, \dots, s_{19} = -9$. Then $A = \{-9, -8, \dots, 8, 9\}$. The series of correlation symbols S is obtained by mapping A into S , where each term of S belongs to A . Combined with Eq. (2), we have that any term s_i of S is represented as,

$$s_i = \begin{cases} 9, & 0.9 \leq r_i \leq 1 \\ 8, & 0.8 \leq r_i < 0.9 \\ \dots \\ 1, & 0.1 \leq r_i < 0.2 \\ 0, & -0.1 < r_i < 0.1 \\ -1, & -0.2 < r_i \leq -0.1 \\ \dots \\ -8, & -0.9 < r_i \leq -0.8 \\ -9, & -1 \leq r_i \leq -0.9 \end{cases} \quad (3)$$

where $A = \{-9, -8, \dots, 8, 9\}$ is interpreted as a scale of correlation levels, with 0 representing insignificant correlation and 9 and -9 representing the strongest positive and negative correlations respectively. Other symbols are similar.

Let a pattern vector $\mathbf{v}_i = (s_i, \dots, s_k)$ represent the dynamic structure of correlation fluctuations within a system of time series. A pattern vector \mathbf{v}_i is constructed from a portion of the correlation symbol series S . This vector \mathbf{v} serves as a representation in the pattern vector space for a point in the reconstruction space by using phase space reconstruction based on the coarse-grained approach.

We define the dimension of the pattern vector as a natural number α . Then the pattern vector is represented as $\mathbf{v}_i = (s_i, s_{i+1}, \dots, s_{i+\alpha-1})$.

Because of the time-order of the correlation symbol series S , the pattern vectors derived from S have their own time-orders, too. The subsequent vector after \mathbf{v}_i is represented as $\mathbf{v}_{i+1} = (s_{i+1}, s_{i+2}, \dots, s_{i+\alpha})$. As a result, we can obtain a series matrix of the correlation patterns $P = (\mathbf{v}_i, \mathbf{v}_j, \dots, \mathbf{v}_k)$ from the series of correlation symbols S by a mapping $g : S \rightarrow P$. We observe that the vectors \mathbf{v}_i and \mathbf{v}_{i+1} with their time-orders have $\alpha - 1$ identical states, denoted by $s_{i+1}, s_{i+2}, s_{i+3}, s_{i+\alpha-1}$. It is convenient for the construction of a network to have such a construction above.

2.1.3. To establish the transition networks

The nodes in a transition network correspond to discrete points in the pattern vector space. If the empirical probability of one node following another along the observed trajectory of the system is non-zero, then a directed edge between them is established. In other words, if the pattern vectors in the reconstructed phase space are considered as the corresponding nodes of the network, then the edges can be established based on the pattern vectors with the time-order.

Let $G = (V, E, \omega)$ be a directed weighted network with its node set $V = \{\mathbf{v}_1, \mathbf{v}_2, \dots, \mathbf{v}_N\}$ and edge set $E \subseteq V \times V$, respectively. Let e_{ij} represent the edge from the node i to the node j , and ω_{ij} be the weight of the edge e_{ij} . The correlated fluctuation system is represented by the network (Fig. 1E), which is formed by arranging pattern vectors from time series. An edge $e_{i(i+1)} = (\mathbf{v}_i, \mathbf{v}_{i+1})$ is a directed edge from \mathbf{v}_i to \mathbf{v}_{i+1} . The network can contain self-edges $e_{ii} = (\mathbf{v}_i, \mathbf{v}_i)$. In this case, its weight is defined by the multiplicity of edges.

2.2. Analysis methods on network

2.2.1. To analyze the correlation fluctuation network by statistics methods

We need to describe some basic statistical properties of a correlation fluctuation network in order to study the underlying dynamical structure of these networks in a normative way. The basic properties of correlation fluctuation networks can be measured by their statistical indicators. The basic properties of the network are clarified by typical statistical indicators such as degree distribution, node strength, clustering coefficient, diameter of network, and average path length.

In a directed network, the in-degree k_i^{in} denotes the number of edges pointing to node i , while the out-degree k_i^{out} denotes the number of edges pointing from node i to other nodes. The degree k_i of node i is defined as the sum of its indegree k_i^{in} and outdegree k_i^{out} , that is,

$$k_i = k_i^{\text{in}} + k_i^{\text{out}} \quad (4)$$

Its degree distribution p_k is the probability of randomly selecting a node of degree k on the network. In general, p_k is estimated using the frequency of n_k as a proportion of n , that is,

$$p_k = \frac{n_k}{n} \quad (5)$$

where n_k is the number of nodes with degree k , and n is the total number of nodes.

The connectivity of node i can be computed by summing the weights of all edges connected to node i . The strength of node i , denoted by $t(i)$, is defined as,

$$t(i) = \frac{\sum_{j \in N_i} \omega_{ij}}{\sum_{i,j \in V} \omega_{ij}} \quad (6)$$

where N_i denotes the neighbourhood set of i , and ω_{ij} is the weight of node i to node j .

Weighted clustering coefficient is a measure of the aggregation and importance of a node in a weighted directed network. It is defined as follows (Saramaki et al., 2007),

$$C^\omega(i) = \frac{1}{\sum_{q \in N_i} \omega_{iq} (k_i - 1)} \sum_{j,k} \frac{(\omega_{ij} + \omega_{ik})}{2} a_{ij} a_{jk} a_{ki} \quad (7)$$

where k_i is the degree of node i , and a_{ij} , a_{jk} , and a_{ki} are indicators of whether nodes i , j , and k form a triangle, where $a_{ij} = 1$ if there is an edge between i and j , and 0 otherwise.

The diameter of a network is an important parameter of its connectivity. It is defined as the maximum length of all shortest paths between any two nodes on the network. The diameter D of a network is defined as,

$$D = \max_{i,j \in V} d(i,j) \quad (8)$$

where $d(i,j)$ is the length of the shortest path between nodes i and j on the network.

The average path length of a network is defined as the average of lengths of all shortest paths between all pairs of nodes in a network.

For a network containing n nodes, the average path length $\langle d \rangle$ is defined as,

$$\langle d \rangle = \frac{\sum_{i,j \in V} d(i,j)}{n(n-1)} \quad (9)$$

where $d(i,j)$ is the length of the shortest paths between nodes i and j .

2.2.2. To analyze the transformation rules in correlation patterns

In a complex network, the approach of community detection identifies the subset of nodes that are more closely connected to each other than to the rest of the network. These subsets, called the communities, can be used to represent functional or structural units within the network. We use clique-based methods to discover smaller, tightly connected communities, and the approach of Girvan-Newman clustering to identify larger, more loosely connected communities. They are crucial for us to unravel the rules of transformation fluctuation in the correlated fluctuation system.

A clique is a subgraph, where every vertex of the subgraph is directly connected to every other vertex in the subset. A k -clique refers to a clique with n vertices (Fig. 2) (Takemoto et al., 2007). It serves as a tool for understanding the global structure of highly connected subgraphs. K-cliques can be used to analyze the structure and functionality of the network. In the correlated fluctuation network, the detection of k -cliques reveals the rule of dynamic patterns within the network.

The Newman-Girvan algorithm is a widely used method for detecting communities in a complex network (Bickel and Chen, 2009). The method identifies communities with higher connectivity between nodes than any other communities of nodes.

The method iteratively removes edges with the highest betweenness centrality, which is the number of shortest paths that pass through each edge. As edges are removed, the network breaks down into smaller components that can be interpreted as communities or modules. This process continues until all edges have been removed, resulting in the decomposition of the network into its constituent communities (Fig. 3).

2.2.3. Key patterns of climate transition on the network

In the real-world networks, the network properties is often influenced by a small fraction of key nodes, the addition or removal of which would significantly improve or degrade certain network properties. We use the algorithm of PageRank ranking to identify the most attractive nodes, while using the theory of structural holes and betweenness centrality to identify nodes that occupy key positions in the transitions of the correlated fluctuation system.

The PageRank ranking is a recursive algorithm that measures the importance of a node by summing the weights of its incoming links. The algorithm starts with a random node and iteratively computes the importance of nodes in a directed weighted network by following links to other nodes. Once the topology of the network (the connectivity relationships) is determined, the PageRank values of the nodes are computed. By calculating the PageRank values of nodes, it is possible to understand the degree of connectivity and the distribution of importance between nodes on the network. The PageRank value of a node reflects its attractiveness and connection strength on the network, which helps us to discover which type of nodes are more likely to move to the patterns of correlated fluctuation network (Gleich, 2015).

The theory of structural holes in a network explains the importance of nodes that occupy bridge positions between different communities. These key nodes have a distinct advantage because they control crucial paths of pattern transitions.

The constraint coefficient serves as an important metric for measuring structural holes. The smaller the constraint coefficient of node i , the more likely it is to become a key node, thus increasing its influence. The constraint coefficient is defined as follows (Hu and Mei, 2018),

$$c(i) = \sum_{j \in N_i} \left(\tilde{\omega}_{ij} + \sum_{q \in N_j} \tilde{\omega}_{iq} \tilde{\omega}_{qj} \right)^2, \quad q \neq i, j \quad (10)$$

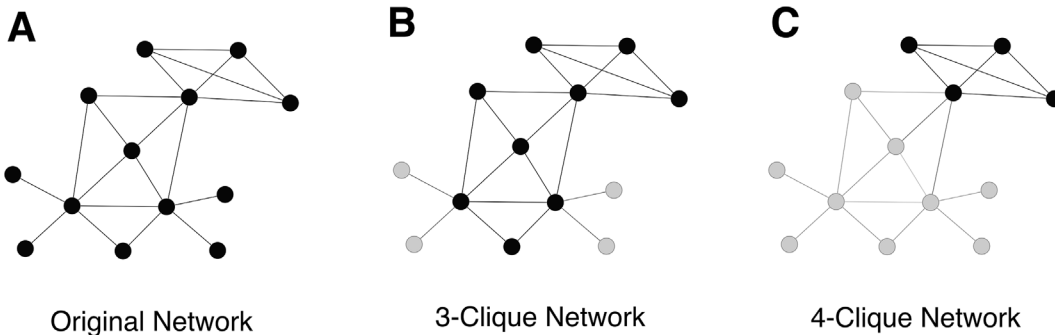


Fig. 2. Let (A) be the original network. (B) and (C), when $k = 3$ or $k = 4$, are shown as black nodes connected by black edges. Each node must be contained in a k -vertex complete subgraph.

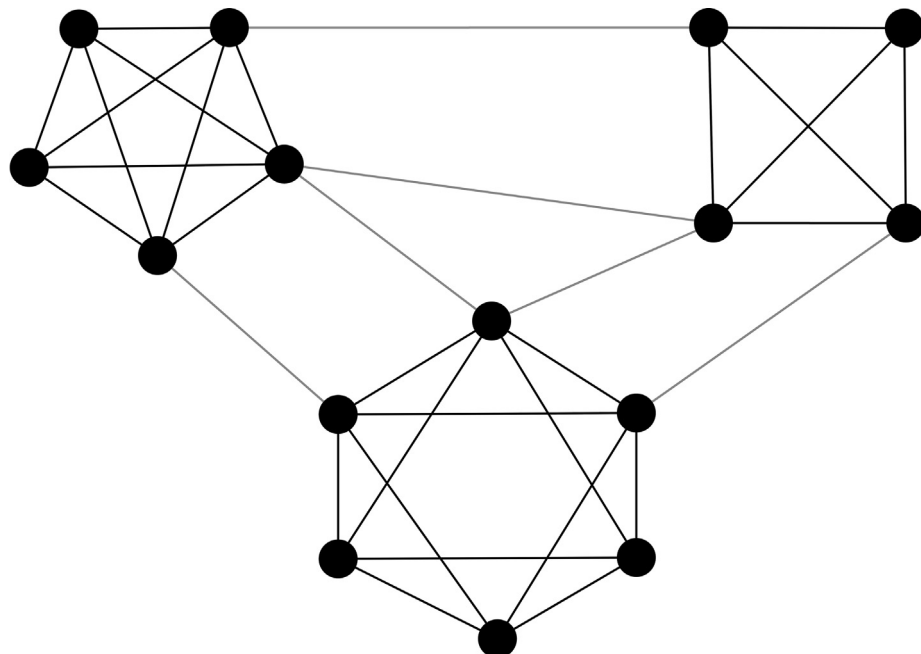


Fig. 3. Within communities, nodes are densely connected, while nodes in different communities are sparsely connected. The original network separates into three independent subgraphs when the edges with the highest centrality are removed. These three subgraphs represent the three communities within the network.

where $\tilde{\omega}_{ij}$ is the normalized mutual weight of the directed edges joining node i and node j . The mutual weight of node i and node j is the sum of the weights of edges joining them.

Betweenness centrality measures the importance of a node in connecting other nodes by shortest paths, or the ability of a node to act as a bridge or intermediary in a network.

Let $d_i^{(st)}$ be the number of all shortest paths from node s to node t passing through i , and n_{st} be the total number of shortest paths from s to t . Then the betweenness of node i is (Brandes, 2001),

$$b(i) = \frac{\sum_{s < t} \frac{d_i^{(st)}}{n_{st}}}{\frac{1}{2} n(n-1)}, \quad s, t \in V \quad (11)$$

where n is the total number of nodes on the network.

3. Data material

Westerhold et al. (2020) presented a new high-fidelity Cenozoic Global Reference benthic foraminifer carbon and oxygen Isotope Dataset (CENOGRID) spanning the past 66 million years. The record

was created by combining data from 14 ocean drilling sites in the Atlantic and Pacific Oceans and has a temporal resolution of 2 kyr for the younger interval and 4.4 kyr for the older interval. After performing binning and resampling operations on the data, they obtained data with intervals of 2 kyr (from 34.026 to 0 Ma) and 5 kyr (67.100 to 34.030 Ma). This documents the overall global carbon and oxygen isotope evolution in the Cenozoic.

These authors discuss some potential biases in the record, such as the uneven distribution of data in space and time, and the perception that thermal gradients within the deep-sea were greater than today. They avoid some biases in the record by using a non-parametric LOESS quadratic regression smooth with a tricube locally-weighted function equivalent to a 20-kyr smooth window. This allowed them to significantly reduce temporal constraints (sampling density), but not regional distribution and water depth biases, a major concern for future scientific ocean drilling.

Currently, the CENOGRID is the most suitable recorder of global temperature/ice volume and global mean carbon cycle. It records accurate data on the correlation fluctuations between $\delta^{13}\text{C}$ and $\delta^{18}\text{O}$ values of the Cenozoic climate system.

4. Main results

We examined the dynamics of the correlated fluctuation system between the carbon ($\delta^{13}\text{C}$) and oxygen ($\delta^{18}\text{O}$) isotopes in the CEN-OGRID. The $\delta^{13}\text{C}$ and $\delta^{18}\text{O}$ isotopes have a weakly negative global correlation coefficient of $r = -0.43$ over the past 66 million years. However, the correlation coefficients between the two time series show a continuous change in the scatter plot (Fig. 4A). The detailed information on the correlation fluctuations of this record will be lost by simply calculating the global correlation coefficients between the two series.

The coarse-grained approach using phase space reconstruction that we constructed the complex network is suitable for representing nonlinear and unstable complex dynamical systems. This approach can show the detailed information of correlation fluctuations, and therefore, it was adopted to represent the correlated fluctuation system between the $\delta^{13}\text{C}$ and $\delta^{18}\text{O}$ isotopes record.

Our objective is to construct nonlinear dynamical systems characterized by low information loss, small time resolution, and robust reliability. The time window determines the time resolution

of the system. Based on general statistical guidelines, we choose a sample size of 40 to calculate the correlation coefficients, i.e. a time window of $l = 40$. During coarse-grained, the properties of the complex network system are determined by the correlation state basis p and the pattern vector dimension α . With increasing number of correlation states and pattern vector dimension, the system granularity becomes finer, while the model stability decreases. Conversely, as the number of correlation states and the pattern vector dimension decrease, the system granularity becomes coarser while the model redundancy increases. In Fig. 4B, we choose a complex network with parameters $(l, p, \alpha) = (40, 19, 4)$ to represent the correlated fluctuation system in order to balance temporal resolution, system stability, and model redundancy. This allows the system to represent important dynamic mechanisms.

This nonlinear dynamical system constructed using the complex network can capture information on a larger scale than the time window l . Therefore, the time window l should be as small as reasonably possible to allow the model to capture more information. The complex network constructed with the current parameters can track the evolution of the correlation with a resolution of

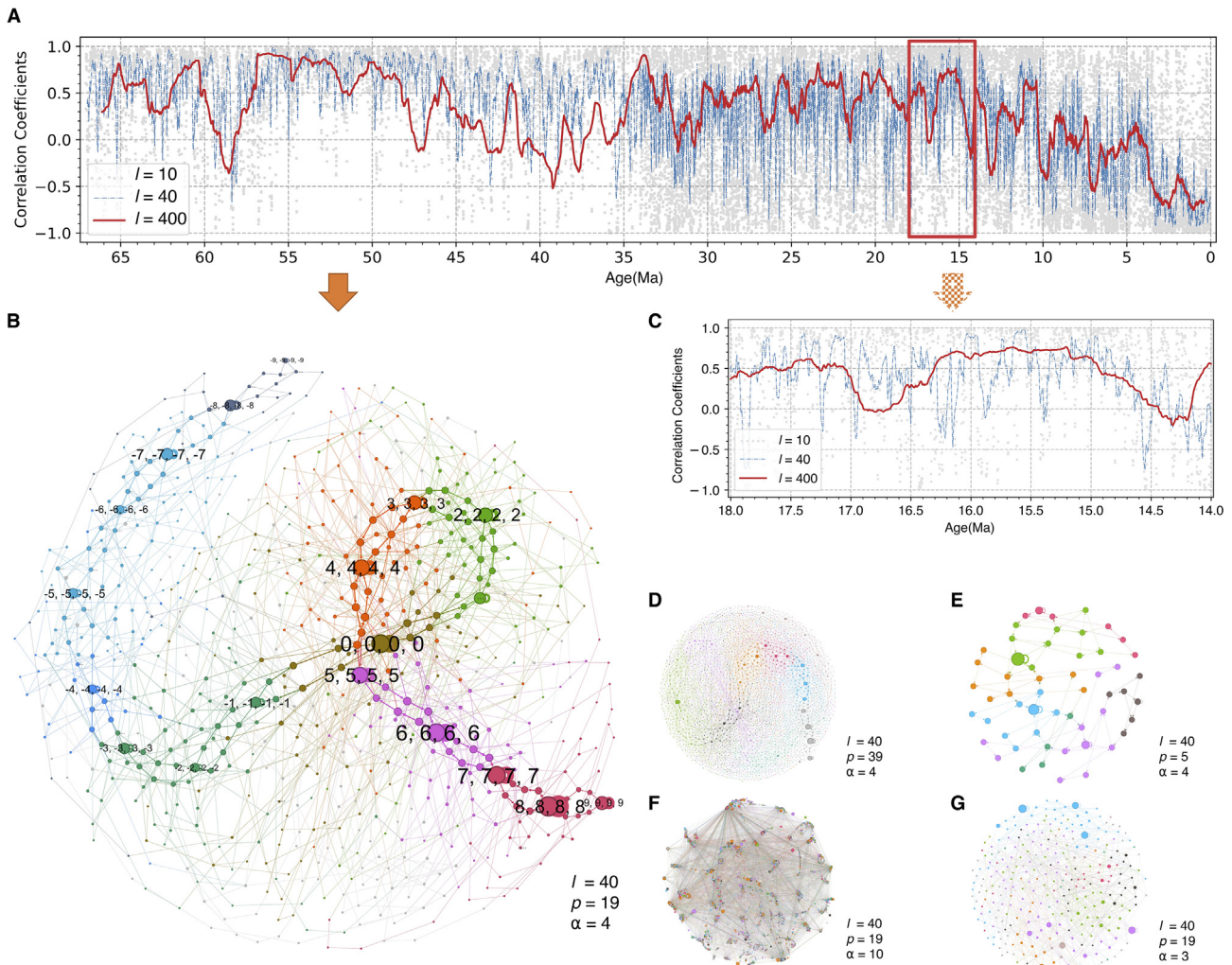


Fig. 4. Correlation fluctuations system under different parameter settings. In (A) different plots of the correlation coefficients are shown for different time scales $l = 10$, $l = 40$, and $l = 400$. The vertical axis represents the correlation coefficients, while the horizontal axis corresponds to time. The complex network constructed with parameters $(l, p, \alpha) = (40, 19, 4)$ is shown in (B). In (C), it can be observed that when the time window $l = 10$ (marked in grey), the time resolution is small but the correlation information cannot be accurately expressed. When the time window $l = 400$ (marked in red), the time resolution is large but most of the correlation information is lost. When the time window $l = 40$ (marked in blue), the correlation information of the system can be retained accurately and non-redundantly. In (D) and (F), larger correlation state basis p or pattern vector dimension α lead to unstable models. In (E) and (G), smaller correlation state basis p or pattern vector dimension α lead to system redundancy, making it difficult to represent detailed information.

he evolution of the correlation with a resolution of 86–215 thousand years, i.e., one symbol is 40 time steps, 4 symbols per pattern $40 + 3 = 43$, so one pattern has 43 symbols. If the interval is 2 kyr, one pattern represents 86 thousand years. If the interval is 5 kyr, one pattern represents 215 thousand years.

In this complex network (the nonlinear dynamical system), weak positive correlations (42.22%) were the most common, followed by no correlations (30.35%). These two types of correlations together accounted for 72.57% of all correlations. Strong negative correlations were the least common, accounting for only 2.41% (Table 1). The network had 687 nodes, which is only 6.87% of the possible total number 10000. This shows that a small number of nodes can represent all the patterns of the correlated fluctuation system.

In such a system, let us consider the distribution of the correlation patterns. We use a widely accepted classification of the Earth's climate during the Cenozoic era, dividing it into four states: the Hothouse, Warmhouse, Coolhouse, and Icehouse (Westerhold et al., 2020). The distribution of the correlation patterns in the different climates is distinct (Fig. 5). In the Hothouse, neither the insignificant correlation patterns nor the negative correlation patterns appear. In the Icehouse, only the negative correlation patterns appear. After the global climate enters the Coolhouse, the number of negative correlation patterns increases significantly. Most of the negative correlation patterns appear after the Eocene–Oligocene Transition. This is because the Eocene–Oligocene Transition marks the transition of the global climate from warm and wet to cold and dry (Zhang and Guo, 2014). Climate change during this period is global, affecting the atmosphere, ocean, and land systems, and thus altering the correlated fluctuation system.

4.1. Metrics on networks

The weighted clustering coefficient of the network was calculated to be 0.015, indicating that the nodes on the network are not closely connected. This result implies that the network is approximately a scale-free network, but not a small-world network. Therefore, it can be concluded that the network has key nodes that control the network.

The diameter and average path length of a network are two metrics that measure its global properties and information transfer efficiency. The diameter of the network is 26, and the average path length is 9.62. This is a slightly smaller diameter and a slightly larger average path length than typically observed in small-world networks. The diameter of the network is about 2.7 times the average path length, indicating that information travels slower between communities on the network, but faster within communities.

The degree distribution of the network is shown in Fig. 6. The cumulative proportion of degrees from 2 to 6 is 86.2%. The point strength of the network was calculated and it was found that a few nodes have a high point strength (Fig. 6B). The log-linear regression curves of the degree distribution and the point strength were fitted separately. It can be seen that the fit of the degree distribution is worse than the fit of the point strength (Fig. 6C, D). The Kolmogorov–Smirnov test (Fasano and Franceschini, 1987) was applied to the metrics to test whether they follow the power law distribution. The K-S test result of the degree distribution was $p = 0.08$, and the test result of the point strength was $p \approx 0$. Although the K-S test of the degree distribution was not significant, it is approximately power-law distributed. The node strength distribution follows a power-law distribution.

4.2. Correlation patterns on networks

K -cliques can identify small, densely connected communities or groups on the network. The method of K -cliques was used to find all structures of the K -clique. Among these structures, 26 3-cliques were identified, but no 2-cliques or 4-cliques and higher were found.

The correlated fluctuation network is a complex system with a topological structure based on 3-cliques. These 3-cliques can be grouped into 19 independent connected subgraphs (Fig. 7A). These subgraphs represent cliques ranging from strong negative correlation to strong positive correlation. All subgraphs have a number of 84 triangles, and the clustering coefficient of the subgraphs is 0.526, indicating that the subgraph network has a high stability.

The weight represents the runtime of the subgraph in the system. In Fig. 7B, the 18th subgraph has the highest weight, indicat-

Table 1

The distribution of correlation symbols in the correlated fluctuation system. A total of 19 symbols from -9 to 9 are used to represent the correlation strength of the 19 intervals of $[-1, 1]$. The correlation strength is explained by a five-level division from strong negative correlation to strong positive correlation. It can be seen that the system is dominated by weak positive correlation symbols and insignificant correlation symbols.

Correlation symbol	Correlation coefficient	Proportion	Correlation symbol	Correlation coefficient	Proportion
9	[0.9, 1]	2.86%	Strong Positive Correlation	[0.8, 1]	11.00%
8	[0.8, 0.9)	8.14%			
7	[0.7, 0.8)	7.94%			
6	[0.6, 0.7)	9.29%			
5	[0.5, 0.6)	8.74%	Weak Positive Correlation	[0.3, 0.8)	42.22%
4	[0.4, 0.5)	8.78%			
3	[0.3, 0.4)	7.47%			
2	[0.2, 0.3)	7.25%			
1	[0.1, 0.2)	5.74%			
0	(−0.1, 0.1)	9.09%	Insignificant Correlation	(0.3, −0.3)	30.35%
−1	(−0.2, −0.1)	4.65%			
−2	(−0.3, −0.2)	3.62%			
−3	(−0.4, −0.3)	3.75%			
−4	(−0.5, −0.4)	2.72%			
−5	(−0.6, −0.5)	2.48%	Weak Negative Correlation	(−0.8, −0.3]	14.01%
−6	(−0.7, −0.6)	2.20%			
−7	(−0.8, −0.7]	2.86%			
−8	(−0.9, −0.8)	2.05%	Strong Negative Correlation	[−0.8, −1]	2.41%
−9	[−1, −0.9]	0.36%			

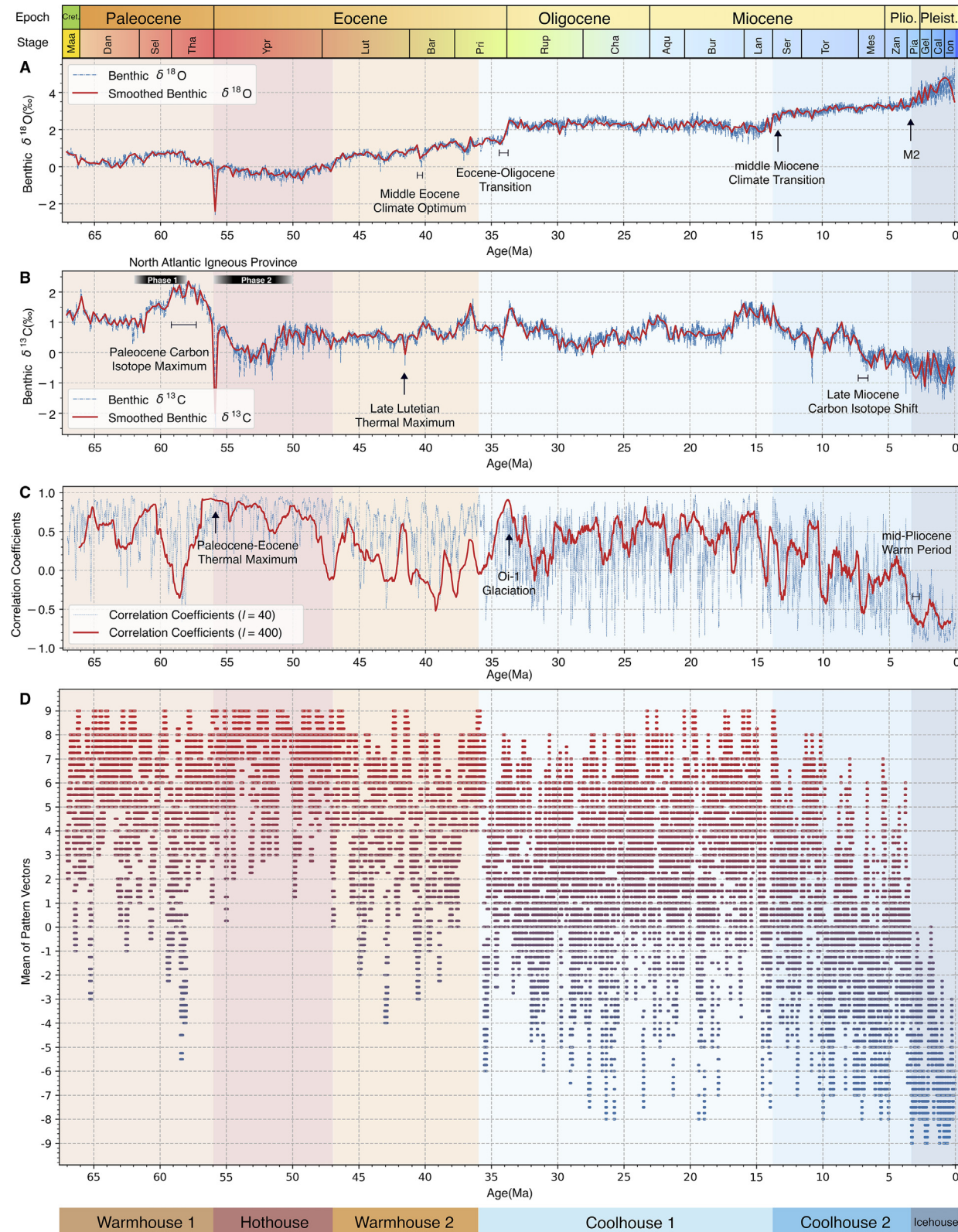


Fig. 5. Benthic $\delta^{18}\text{O}$ and $\delta^{13}\text{C}$ records from the CENOGRID. (A) benthic $\delta^{18}\text{O}$, (B) benthic $\delta^{13}\text{C}$, (C) correlation coefficients, and (D) mean of pattern vectors. In (D) we use the parameters of $(l, p, \alpha) = (40, 19, 4)$. The smoothing method for (A)(B) is cubic spline interpolation. The strength of the correlation patterns is indicated by the mean value of the pattern vectors. For example, the average pattern vector of $(-9, -8, -7, -6)$ is -7.5 , indicating a weak negative correlation. The colours of the correlation patterns range from red to blue, indicating the correlations from positive to negative. The different coloured backgrounds represent four different states of the Earth's climate during the Cenozoic. The drawing method is referenced from Westerhold et al. (2020). Cret., Cretaceous; Plio., Pliocene; Pleist., Pleistocene; M2, first major glacial event in the northern hemisphere; Oi-1, the first major glacial period in the Oligocene; Cret., Cretaceous; Plio., Pliocene; Pleist., Pleistocene; Maa, Maastrichtian; Dan, Danian; Sel, Selonian; Tha, Thayanian; Ypr, Ypresian; Lut, Lutetian; Bar, Bartonian; Pri, Priabonian; Rup, Rupelian; Cha, Chattian; Aqu, Aquitanian; Bur, Burdigalian; Lan, Langhian; Ser, Serravallian; Tor, Tortonian; Mes, Messinian; Zan, Zanclean; Pia, Piacenzian; Gel, Gelasian; Cal, Calabrian; Ion, Holocene.

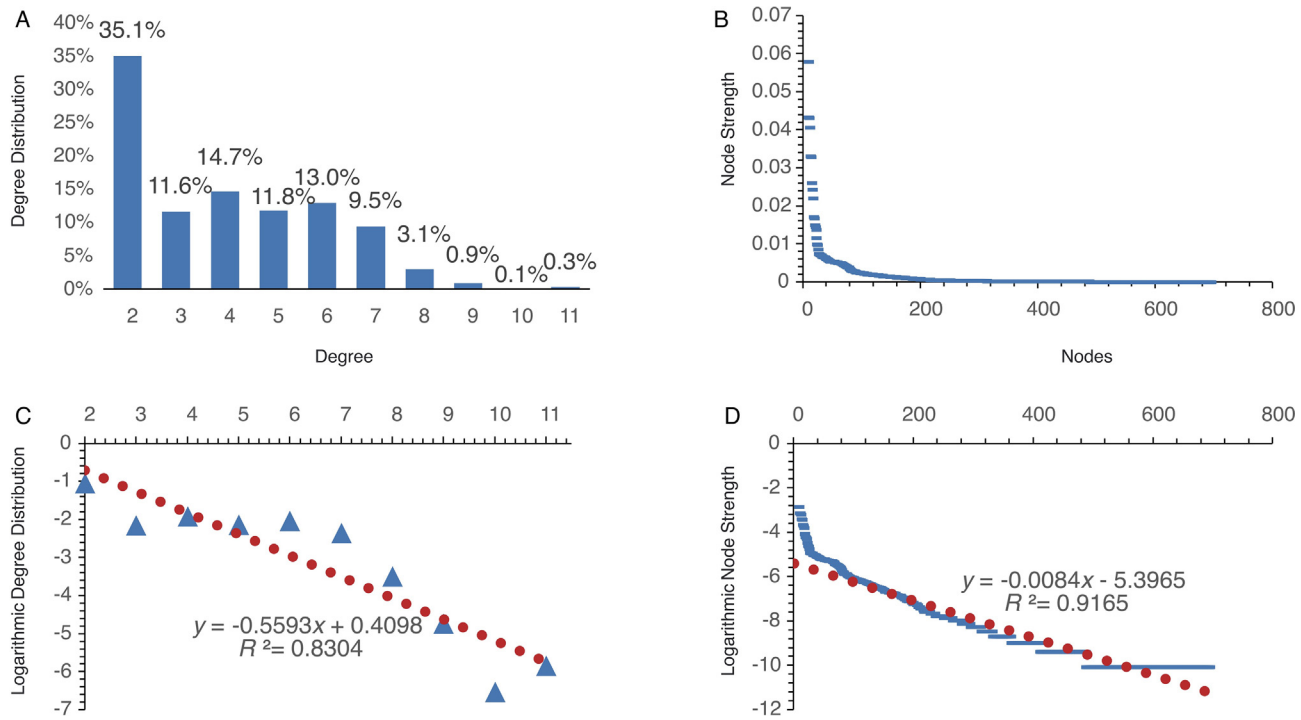


Fig. 6. The degree distribution and node strength distribution of the network both follow a power law. (B)(D) The logarithmic regression curve of the point strength fits well, with an R^2 of 0.92. (A)(C) The degree distribution fits less well, but the R^2 is still high at 0.83. This indicates that 92% of the log distribution of dot strength can be explained by the logarithmic regression curve, and 83% of the log distribution of degree can be explained by the logarithmic regression curve.

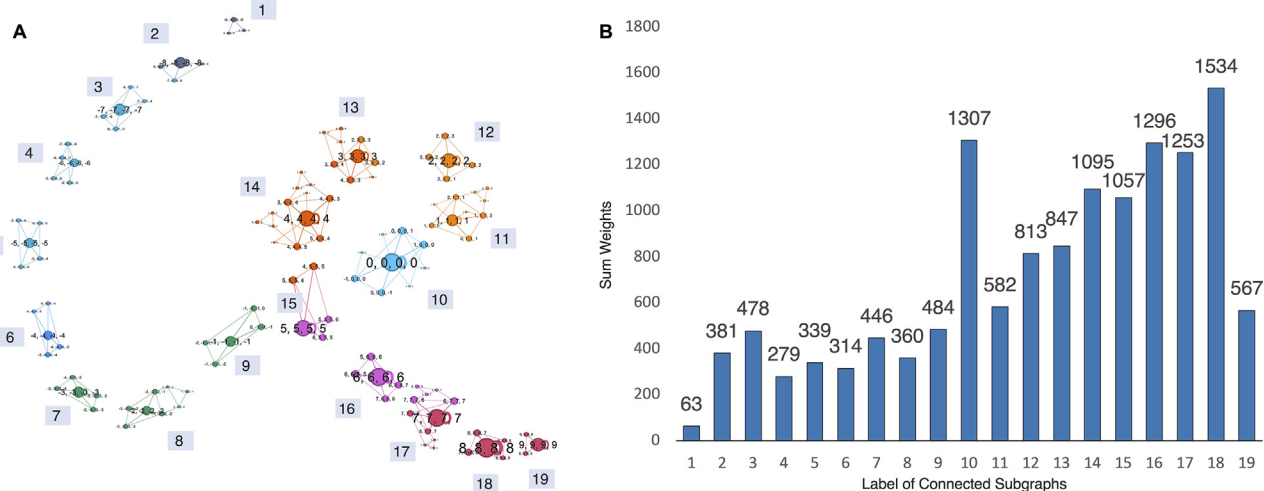


Fig. 7. 19 connected subgraphs based on 26 3-cliques. (A) The correlated fluctuation network contains 26 3-cliques and 19 connected subgraphs. These connected subgraphs are labelled in order from negative to positive correlation. (B) shows the sum of the weights of the connected subgraphs. In the correlated fluctuation network, the sum of the weights of a subgraph represents the runtime of the correlated fluctuation network on that subgraph.

ing that the 18th subgraph plays a key role in the network. All 3-cliques show a left skew, indicating that positive correlation has played a leading role in the correlated fluctuation system since 66 Ma.

The Newman-Girvan algorithm is a powerful graph partitioning algorithm that can detect larger communities in a network. In Fig. 8, the results showed that the network has strong communities (maximum modularity found: 0.7). The algorithm finds a total of 17 communities. After sorting them by the number of nodes, we select the 9 communities with the largest number of nodes. These 9 communities account for 85% of the total number of nodes, 73%

of the total number of edges and 99.35% of the total weight. The remaining communities are classified as community 10.

4.3. Key nodes on networks

We computed the PageRank values, the betweenness centrality and the constraint coefficients of structural hole of the network nodes to investigate which nodes have control power in the network. The power-law distribution of the key nodes measure was tested using the log regression curve (Fig. 9). The results showed that the PageRank values, the betweenness centrality and the con-

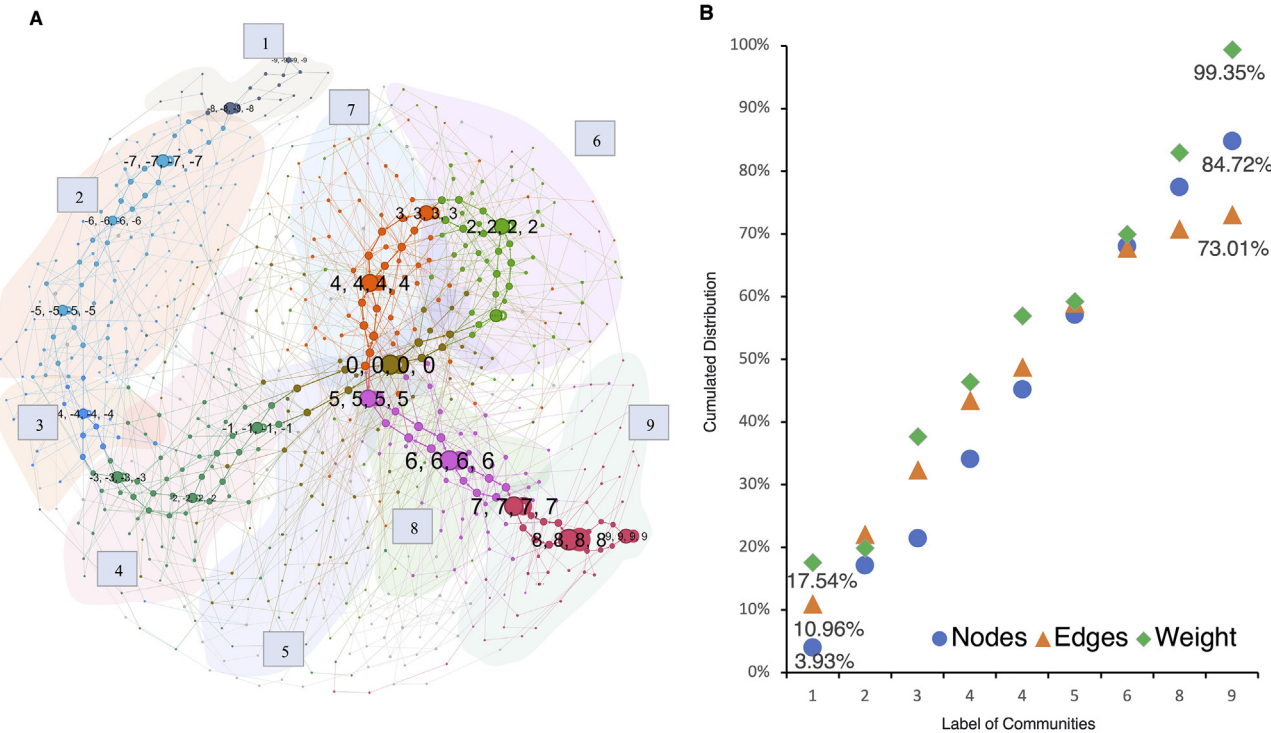


Fig. 8. The graph partition based on the Newman-Girvan algorithm, with different colours representing different community divisions. (A) It can be observed that the correlation represented by communities 1 to 9 gradually increases. Community 10 is shown in grey and is a scattered node that cannot be classified into a community. (B) The vertical axis represents the cumulated distribution of nodes, edges and weights. The horizontal axis represents the communities sorted in ascending order of correlation strength, with community 10 sorted separately. This partition uses 9 subgraphs to represent the main part of the network and has a good performance in community detection.

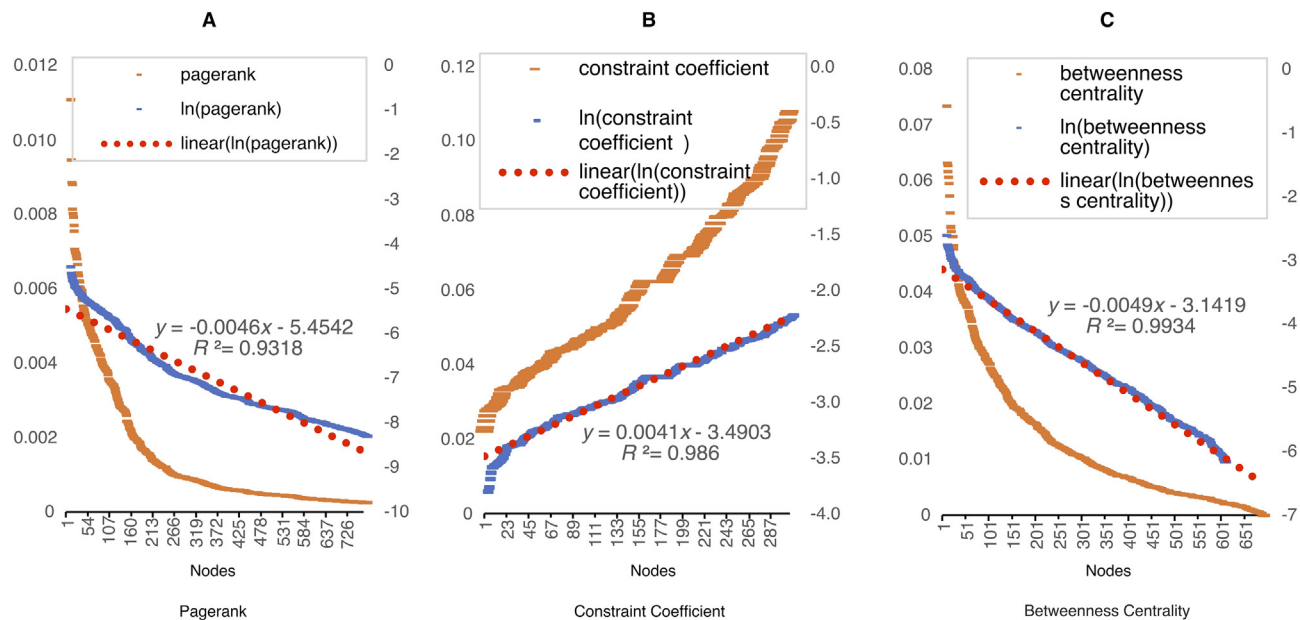


Fig. 9. The key nodes measure of the CENOGRID correlation fluctuation network. (A) and (C) are sorted from large to small, as both the PageRank and the Betweenness Centrality become more effective as the measure increases. (B) is sorted from small to large, as the smaller the constraint coefficient of structural hole, the more likely the node is to become a key structural hole. The three measurements of key nodes fit the log regression curve well. All three measurements have removed invalid tail data to ensure the validity of the log regression curve.

straint coefficients of the network all follow a power-law distribution, indicating that a small number of nodes are in key positions on the network.

The PageRank algorithm is a method for determining which nodes in a network are more likely to be transformed by patterns.

The PageRank values of all nodes sum to 1. By calculating the PageRank values of the network, we found that the distribution of nodes with higher PageRank values on the network is consistent with the distribution of 3-cliques. We also generated networks with nodes whose cumulative PageRank values are in the 5%,

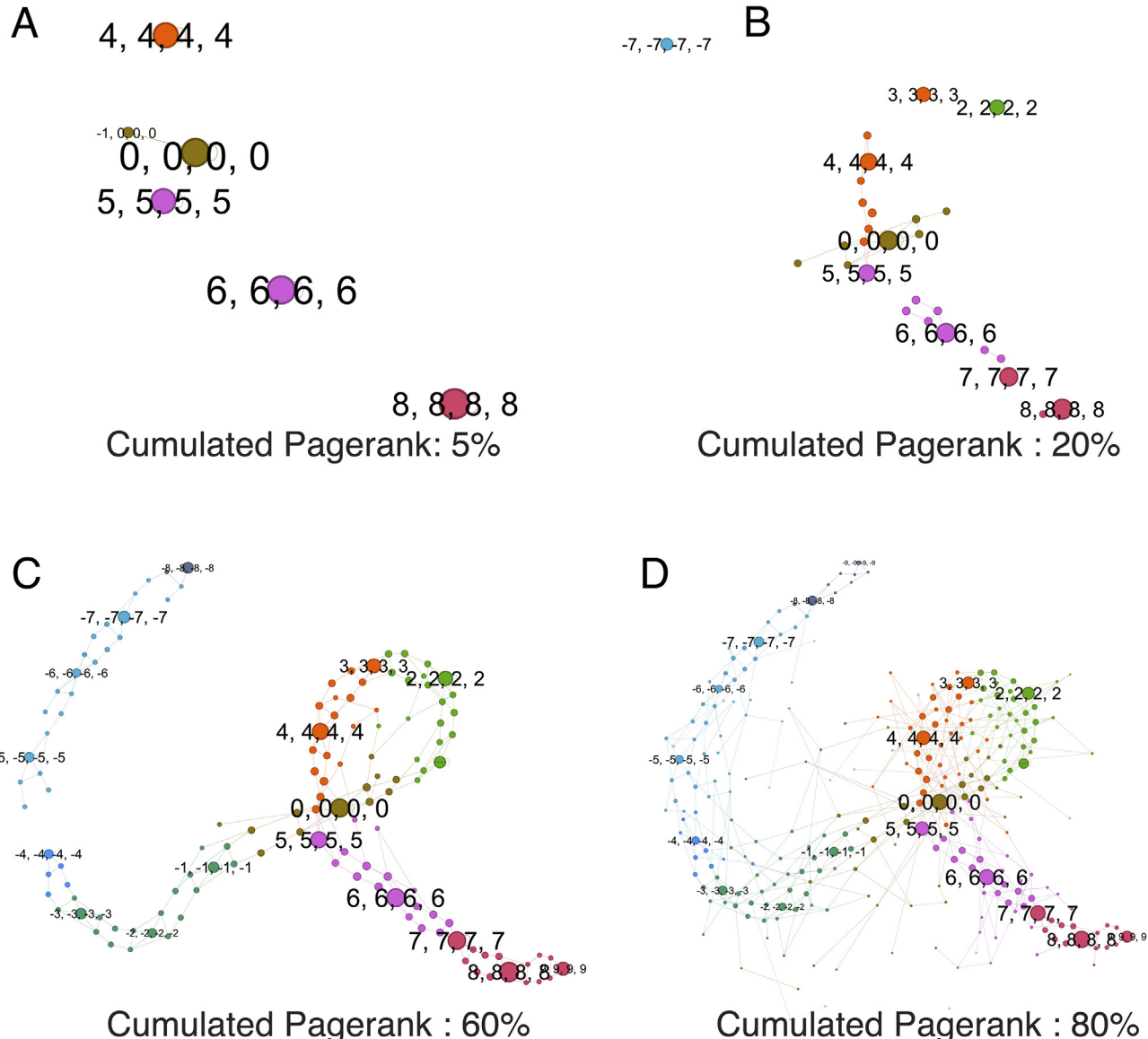


Fig. 10. (A) network of nodes with high PageRank values. (A), (B), (C) and (D) represent the network generated when the accumulated PageRank values are 5%, 20%, 60% and 39.7% of the total number of nodes have an accumulated PageRank value of 80%.

20%, 60%, and 80% quantiles, and found that the generated networks are highly correlated with the subgraphs of 3-cliques.

Fig. 10 shows the cumulative PageRank values of the nodes on the network. Six nodes have a cumulative PageRank value of 5.44%, which is a very high value. These nodes have insignificant correlation patterns (0, 0, 0, 0), weak positive correlation patterns (4, 4, 4, 4), (5, 5, 5, 5), (6, 6, 6, 6), and strong positive correlation patterns (8, 8, 8, 8). These patterns show significant attractors within the correlated fluctuation system.

In the structural hole theory, we postulate that the nodes with small constraint coefficients play a more important role in the pattern transitions. The constraint coefficient measures the control ability of nodes, and the nodes with small constraint coefficients often act as mediators between different patterns. In Fig. 11, three nodes with the smallest constraint coefficients are located in the uncorrelated community (nodes 1, 2, and 4). This implies that the uncorrelated community plays an important role in the pattern transition of the whole network.

Betweenness centrality measures the frequency with which a node appears on the shortest paths between two other nodes. By

controlling nodes with high betweenness centrality, it is possible to control the speed of patterns switching. In Fig. 12, nodes with high betweenness centrality are mainly located in communities with weak negative correlation and strong positive correlation. This implies that these two correlation communities can be used to control the speed of patterns switching by nodes with high betweenness centrality.

5. Conclusion

Using the CENOGRID dataset to construct the network of the correlated fluctuations, we represent the correlated fluctuation system between $\delta^{13}\text{C}$ and $\delta^{18}\text{O}$ series in the Earth system since 66 Ma. The system tracks the changes of correlation series on time scales of 86 to 215 thousand years, inferring the dominant stable modes and key patterns of the climate transition.

This information helps us understand the past climate dynamics and the relationship between the carbon cycle and climate. Our results can be used to improve climate models and predictions

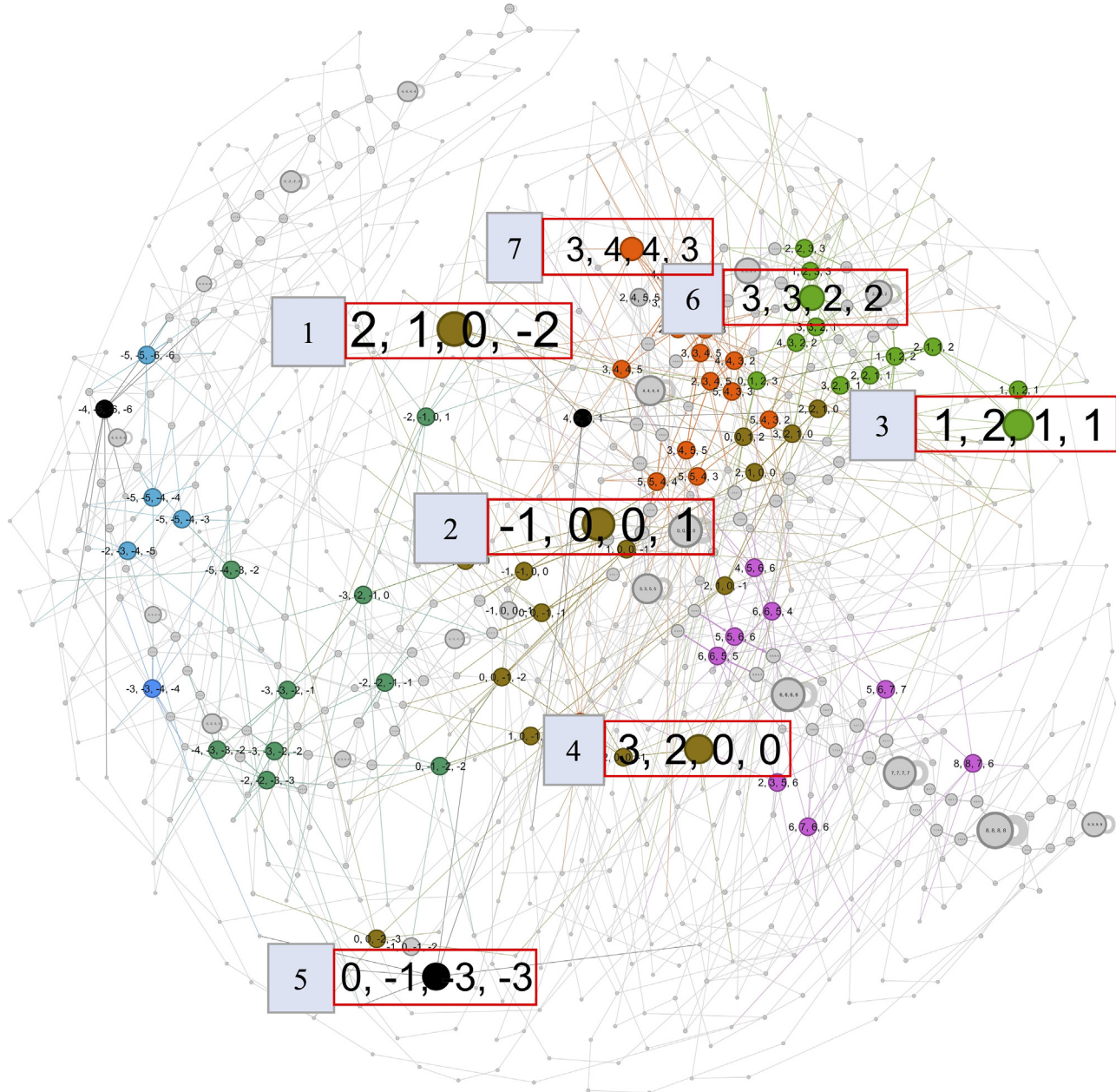


Fig. 11. The network sorted by the structural hole constraint coefficient (descending order). The coloured nodes are the top 10% of nodes. The nodes in the top 1% are labelled with numbers from 1 to 7.

of the future climate change. For example, our results infer that changes in polar ice volume are a key factor in the systematic modulation of $\delta^{13}\text{C}$ and $\delta^{18}\text{O}$ correlations within climate dynamics. Understanding these can help us to better understand the climate change and mitigate its impacts.

5.1. Stable modes in the correlated fluctuation system

The correlation fluctuation system of the CENOGRID is characterized by a scale-free network model. This network model is characterized by a high degree of heterogeneity, with most nodes having a small number of connections and a few nodes having a large number of connections. The absence of 4-cliques or higher community structures in the network indicates that the mode transition between communities is slower than in small-world net-

works. This observation may be attributed to the presence of stable structures in the network, which facilitate rapid node switching within small regions, but impede node switching between large regions.

The network contains 26 3-cliques, which form 19 connected subgraphs (Fig. 7). This means that the system will mainly operate in these subgraphs. These 19 subgraphs represent correlation states from 9 to -9, and the entire correlation system fluctuates around these 19 subgraphs. The correlated fluctuation system will remain in a stable mode in these connected subgraphs. The 19 connected subgraphs account for 17.5% of the total number of nodes, 15.2% of the total number of edges, but 56.4% of the total weight. This means that for 56% of the time since 66 million years ago, the system has operated on these 19 subgraphs (Figs. 7 and 13).

Stable modes are represented by 3 cliques to simplify the study in the complex system. Fig. 13 shows that the 4th and 5th 3-clique

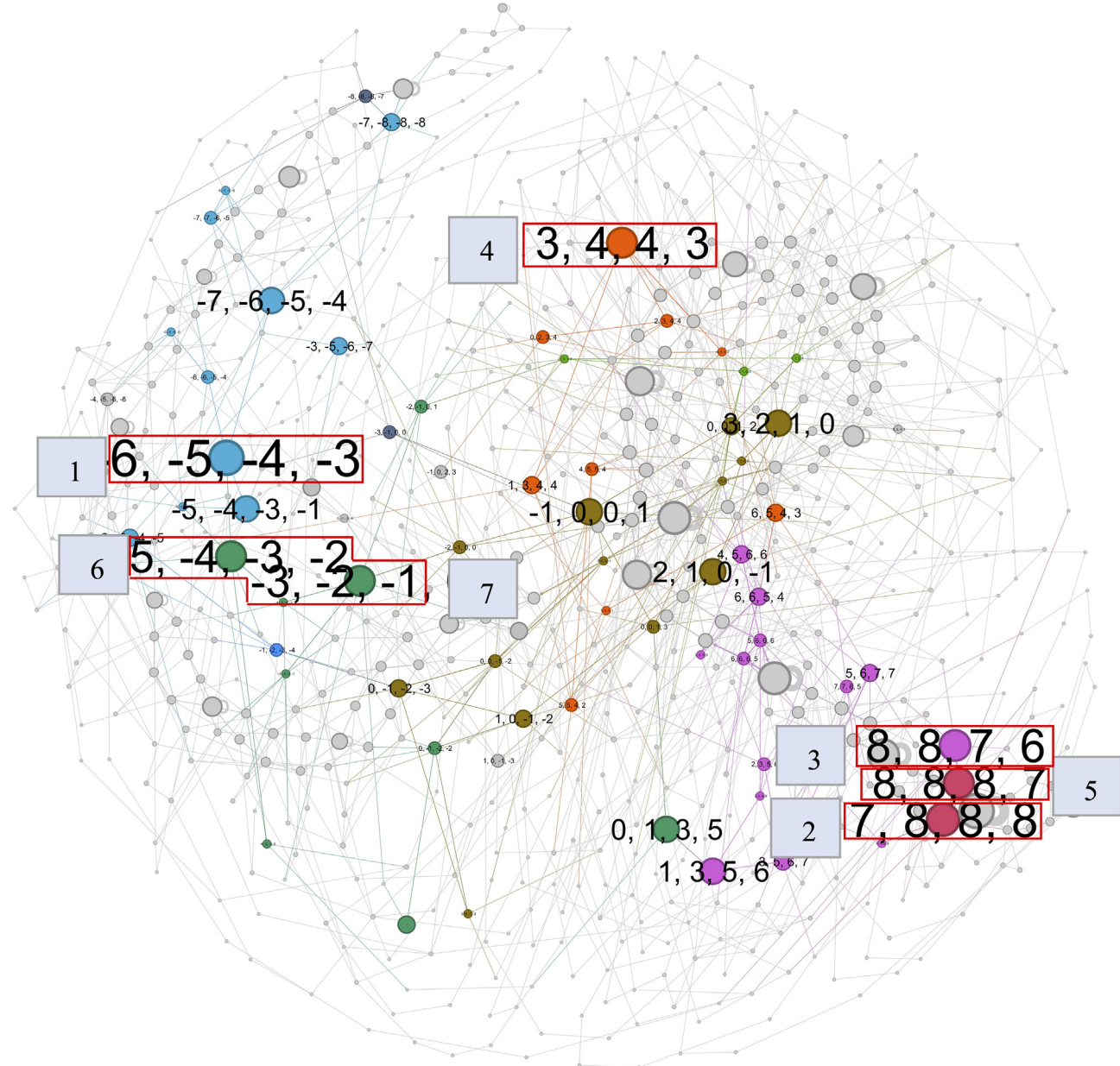


Fig. 12. The distribution of high betweenness centrality nodes on the network. Nodes with betweenness centrality in the top 10% are coloured. Nodes with betweenness centrality in the top 1% are labelled 1 to 7.

(weak negative correlation) appeared at 35.5 Ma, while the 24th 3-clique (weak positive correlation) disappeared at 29.8 Ma. These phenomena are probably related to the appearance of the permanent ice cover that established on Antarctica (Coxall et al., 2005; Okuno and Miura, 2013) and the extinction of large benthic foraminifera during the Eocene-Oligocene transition (Cotton and Pearson, 2011; Basak and Martin, 2013). These results show a significant change in the fundamental dynamics of the correlated fluctuation system of the $\delta^{13}\text{C}$ and $\delta^{18}\text{O}$ during this period. However, the stable modes of the 25th and 26th 3-clique persist during this period, showing that stable modes of strong positive correlation are maintained in this system.

In Fig. 13, after the middle Miocene Climate Transition, the Arctic ice sheet initiated (Bailey et al., 2013; Rohling et al., 2017; Gasson et al., 2018), accompanied by the disappearance of the weak positive correlation 22th 3-clique (11.2 Ma) and the strong positive correlations 25th (11.1 Ma) and 26th (13.6 Ma) 3-

cliques. In contrast, the 2nd (26.4 Ma) and 3rd (27.7 Ma) 3-cliques were activated by the opening and deepening of the Drake Passage gateway, the establishment of the Antarctic Circumpolar Current, and the Wah Wah Springs supervolcano and La Garita Caldera eruptions in Colorado. Those imply that the stable modes of the correlated fluctuation system shifted towards strong negative correlations. After 3.3 Ma, Arctic ice volume increased rapidly and global temperature continued to decrease. This activated the 1st 3-clique (strong negative correlation), marking the system remained stable in negative correlation.

Furthermore, in Fig. 14, the network has been divided into 10 communities using the Newman-Girvan algorithm. The patterns with similar correlations are grouped together. This is a special class of stable modes that have a larger scale than 3-clique structures. The Paleocene-Eocene Thermal Maximum (PETM) (55.93 Ma) was a landmark global warming event that led to major variations in $\delta^{13}\text{C}$ and $\delta^{18}\text{O}$. As a result of the significant climate

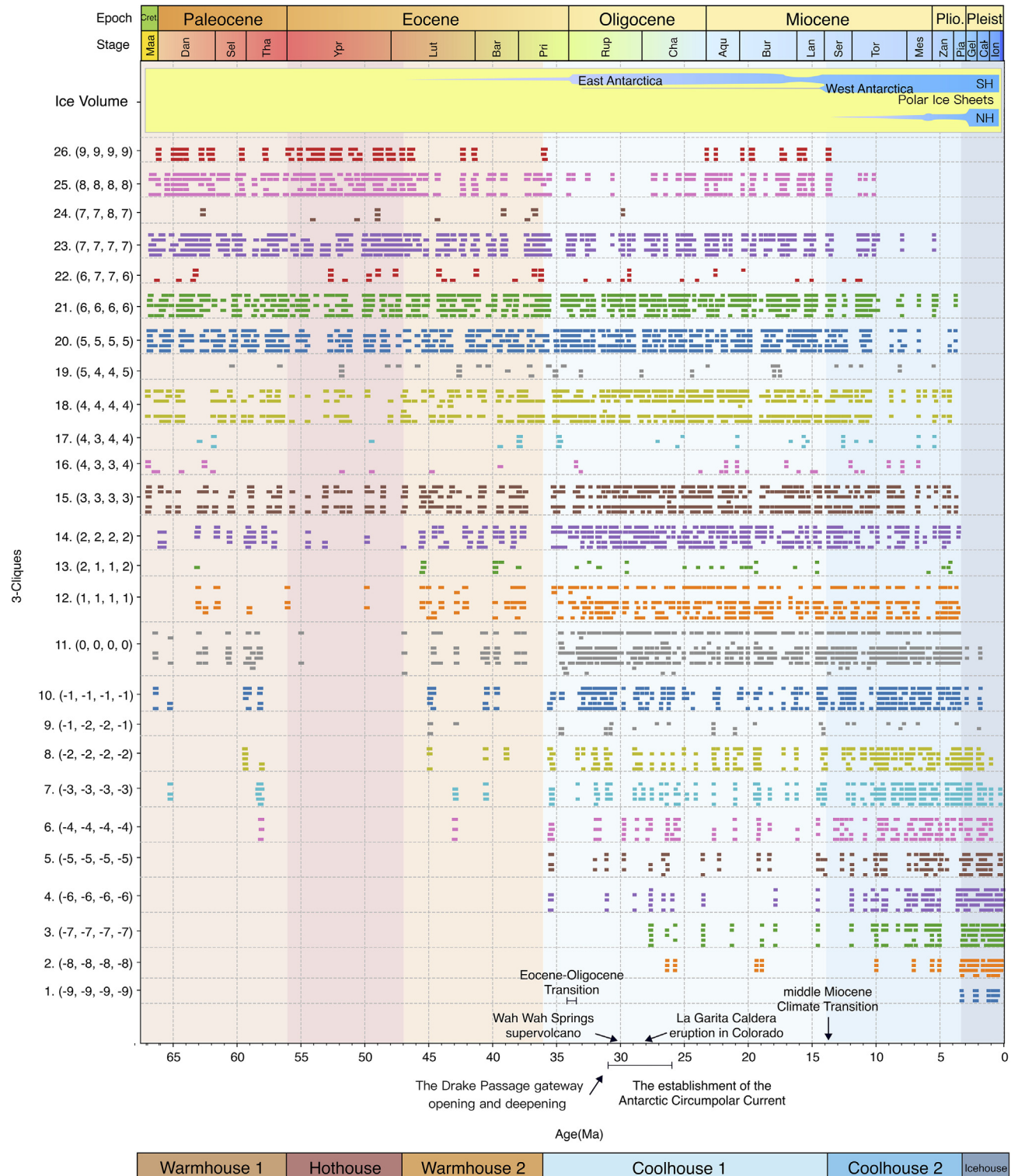


Fig. 13. The spectrum of 3-cliques over time. The vertical axis represents different 3-cliques, and the horizontal axis represents time. The pattern of highest weights in each clique is marked, and the blue horizontal bars give a rough estimate of the ice volume in each hemisphere. Major geological and climatic events are also marked on the graph. The drawing method of ice volume is referenced from Westerhold et al. (2020). SH, Southern Hemisphere; NH, Northern Hemisphere. Other abbreviations used in the figure are explained in Fig. 5.

change, most of the marine plankton, began to disappear and the fluctuation of $\delta^{13}\text{C}$ and $\delta^{18}\text{O}$ values became increasingly complex (Cao et al., 2018; Jolivet and Boulvais, 2021). The Hothouse state, which operated between the PETM to the end of the Early Eocene Climate Optimum, was characterized by high temperatures ($> 10^\circ\text{C}$ above present). During this period, the 1st, 2nd, 3rd, and

4th communities, which represent positive correlations, were not observed. The 5th community, which represents insignificant correlation, was also absent during both the Hothouse and Icehouse.

The M2 (first major glacial event in the Northern Hemisphere) marks the transition from the Coolhouse to Icehouse. During this period, only the 1st, 2nd, 3rd, and 4th communities, which repre-

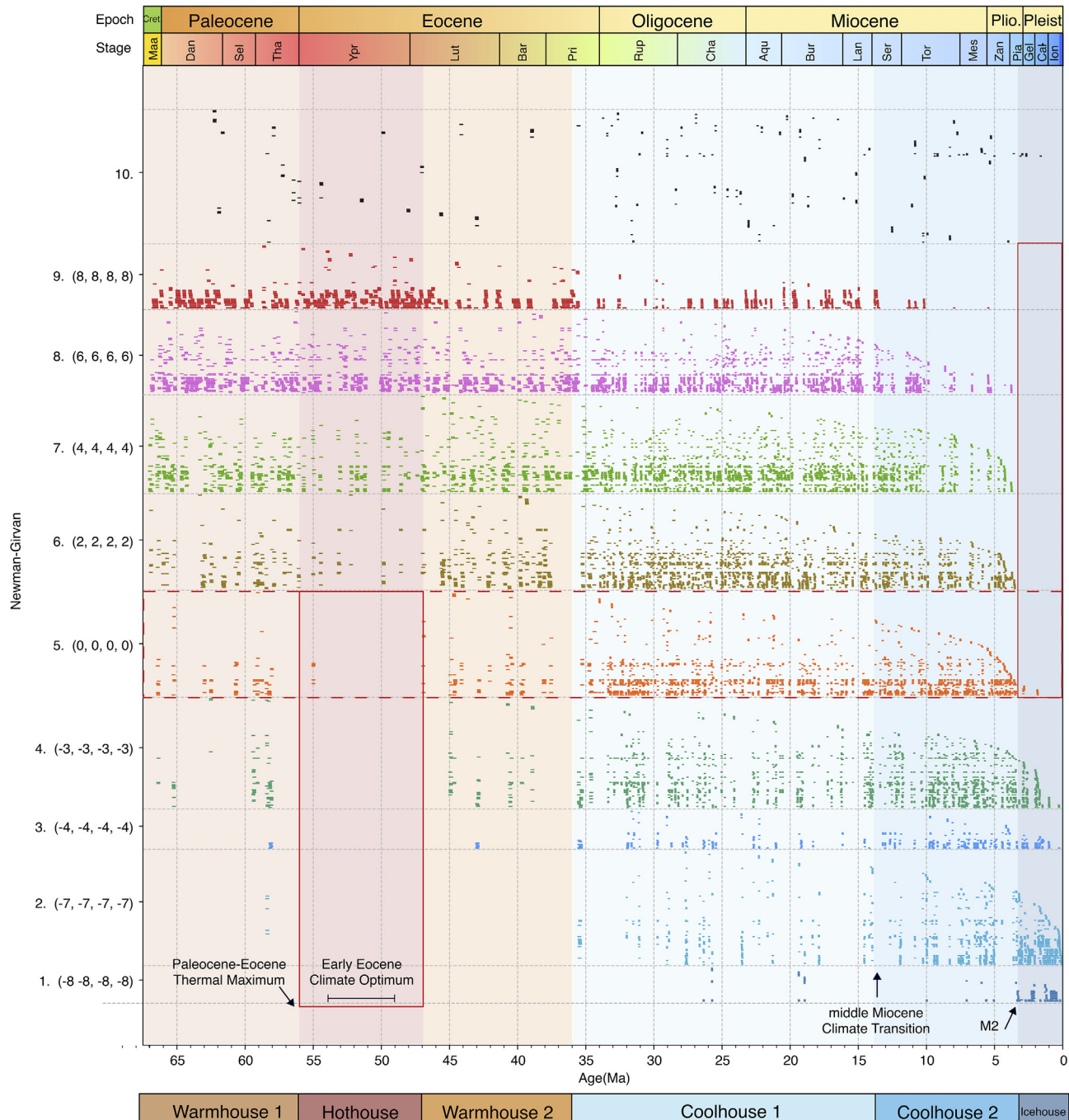


Fig. 14. The spectrum of communities over time. The vertical axis represents different communities, and the patterns with the highest degree in each community are marked. Different colors of the background represent the four different climate states of the Earth's climate during the Cenozoic: hothouse, warmhouse, coolhouse, and coldhouse. The red realization boxes in the figure mark the absence of some communities in the hothouse and coldhouse climate states. The red dashed box marks community 5 with insignificant correlation. Abbreviations used in the figure are explained in Fig. 5.

sent positive correlations, were observed. This indicates the transition of the correlated fluctuation system into a phase dominated by negative correlations. This shift is believed to be driven by polar ice volume in the Northern Hemisphere (Bailey et al., 2013; Turner, 2014). These results suggest the importance of polar ice volume as a primary driver of stable modes transitions in the correlated fluctuation system.

5.2. Climate states impact the stable modes

The Earth's climate system has four fundamental climate states (Westerhold et al., 2020), which are based on how it responds to

astronomical forcing, greenhouse gas contributions, polar ice volume, etc.

Under different climate states, the correlated fluctuation system shows different stable patterns. When the climate was in the Hot-house or Icehouse, the stable modes of the system show mainly positive or negative correlation features (Fig. 15B and D). When the climate was in the Warmhouse, the stable modes of the system are mainly in positive correlation (Fig. 15A). The stable modes of the positive correlation are slightly more common than the others in the Coolhouse state, accounting for 48.3% of the runtime. Insignificant correlation and negatively correlated states account for 37.0% and 14.7%, respectively (Fig. 15C).

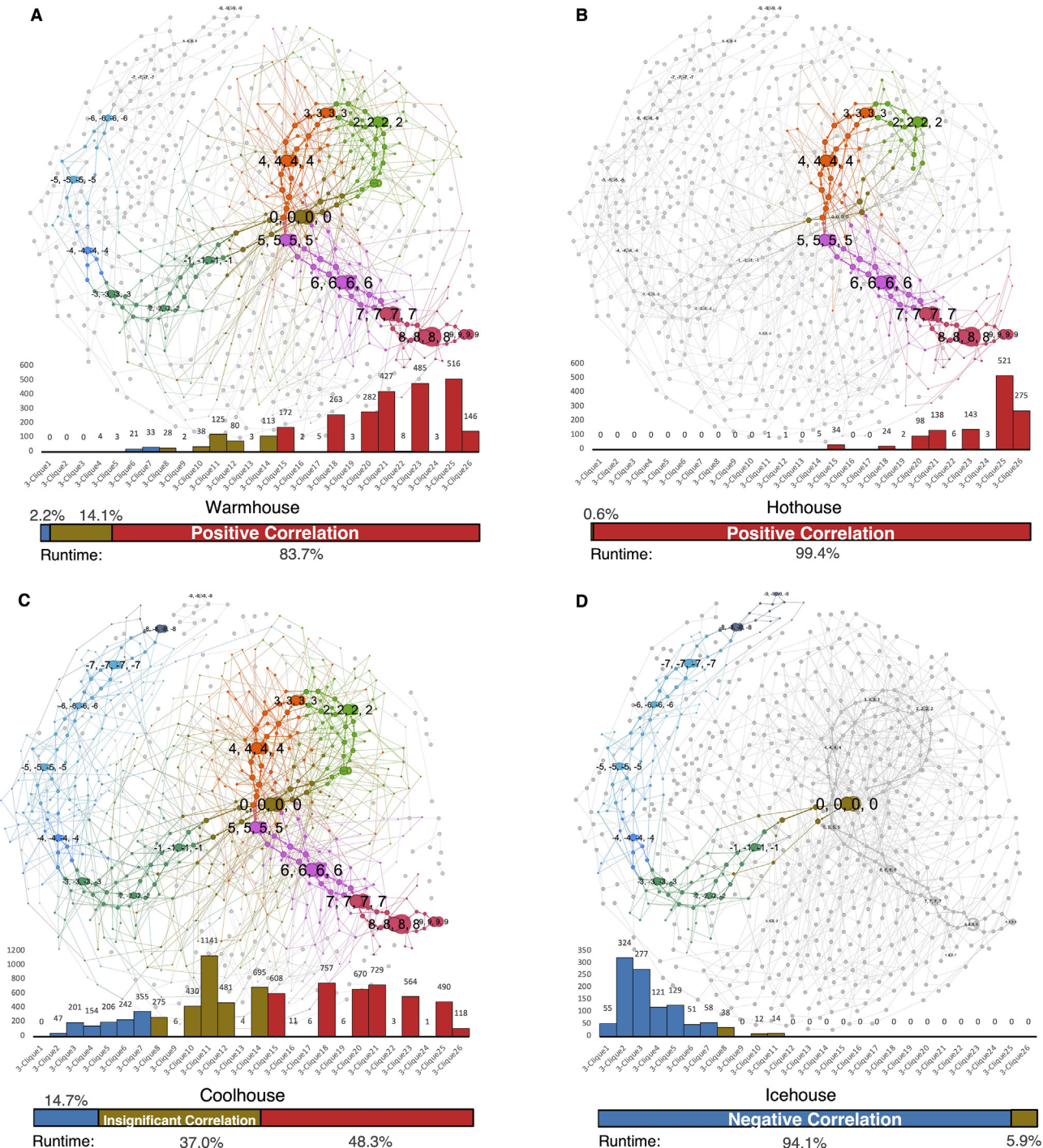


Fig. 15. Networks and 3-clique weight distributions under four climate states. In different climate states, the corresponded patterns run on the coloured networks, and the grey nodes indicate that they are not in the current climate state. The histograms show the weights of 3-cliques in the current climate state, which are proportional to the runtime of 3-cliques on the network. The horizontal axes are colored blue, brown, and red to represent negative correlation, insignificant correlation, and positive correlation, respectively.

The fundamental climate states exerts a profound influence on the stable modes of the correlated fluctuation system. As the climate states shifted to the Coolhouse, a unipolar glacial state was established in Antarctica (Spray et al., 2019), leading the correlated fluctuation system of $\delta^{13}\text{C}$ and $\delta^{18}\text{O}$ to a transition from the positive correlations dominated of the Warmhouse to a diversified correlations of the Coolhouse (Fig. 15A, C). The glaciation of the Northern

Hemisphere began to grow in the late Coolhouse and expanded rapidly in the Icehouse (Bridges et al., 2023). As the Northern Hemisphere glaciation grew, the correlated fluctuation system of $\delta^{13}\text{C}$ and $\delta^{18}\text{O}$ was observed to operate mainly in the stable negative correlation modes. This implies that both different climate states and the polar ice volume have important impact on the stable modes of the system.

5.3. Key patterns of climate transition on the network

The correlated fluctuation system of the $\delta^{13}\text{C}$ and $\delta^{18}\text{O}$ isotopes tends to evolve towards key patterns with higher PageRank values. This is shown in Figs. 8 and 10, where the high PageRank nodes in the network are located in the non-negative correlation communities. As shown in Fig. 16A, the 1st to 7th patterns of high PageRank values are observed for most of the time since 66 Ma, but the 1st and 6th patterns, representing insignificant correlation, do not appear during the Hothouse state. The 25th pattern has the highest PageRank value of all negative correlation patterns, and it appears at 27.6 Ma. This indicates that the correlated fluctuation system began to transition to the weak positive correlation. After entering 10 Ma, the frequency of occurrence of the 25th pattern increased significantly, while the frequency of occurrence of the 2nd, 3rd, 4th, and 5th positive correlation patterns decreased significantly (Fig. 16A). This implies that a fundamental dynamical transition occurred in the global correlated fluctuation system at this time.

In the structural hole theory, the structural hole nodes of small constraint coefficients control the transition of the patterns. In Fig. 11, effective structural hole nodes appear mainly in the insignificant correlation community and the weak positive correlation community. As shown in Fig. 16B, the number of strong structural hole nodes is significantly higher during the periods from 35 Ma to 31.4 Ma and from 11.2 Ma to 8.0 Ma, with more than 5 nodes in each period. Several structural hole nodes contributed to the dynamic changes of the system during the onset and end of the Coolhouse state.

Nodes with higher betweenness centrality have more shortest paths between them and play a more important role in the system of different communities. Therefore, key patterns with high betweenness centrality may be associated with extreme climate changes. Based on the spectral plot of the top 1% of nodes by

betweenness centrality, five or more key patterns with high betweenness centrality were observed four times within the 1 Ma range (Fig. 16C). These correspond to major climate change events, including the North Atlantic Igneous Province, the establishment of the Antarctic Circumpolar Current, the Miocene Climate Optimum, and the Tortonian Thermal Maximum.

Large Igneous Provinces (LIPs) are notable associated in climate perturbations in Earth's history. The North Atlantic Igneous Province (NAIP) played an important role in global warming from the late Paleocene to early Eocene, and the NAIP and PETM are significantly association (Thomas and Bralower, 2005; Jones et al., 2019; Lindsay et al., 2021). In our work, five key patterns with high betweenness centrality appeared (59–58 Ma) (Fig. 16C), during the NAIP. Those show that the NAIP changed the underlying drivers of the correlated fluctuation system during this period. This is closely related to the subsequent PETM and the global climate shift from Warmhouse to Hothouse.

As shown by the nodes with higher betweenness centrality of the system (Fig. 16C), the Earth's underlying dynamical drivers also changed significantly around 27.4–26.4 Ma, 15.4–14.4 Ma, and 10.7–9.7 Ma, respectively. These results corroborate previous associations between these periods and significant climatic events, including the Antarctic Circumpolar Current, the Miocene Climate Optimum, and the Tortonian Thermal Maximum. Notably, these events are all linked to major climate transitions (Hill et al., 2013; Longman et al., 2022; Harzhauser et al., 2023).

CRediT authorship contribution statement

Shifeng Sun: Conceptualization, Investigation, Methodology, Software, Formal analysis, Data curation, Visualization , Writing – original draft. **Haiying Wang:** Supervision, Conceptualization, Investigation, Resources, Methodology, Data curation, Validation,

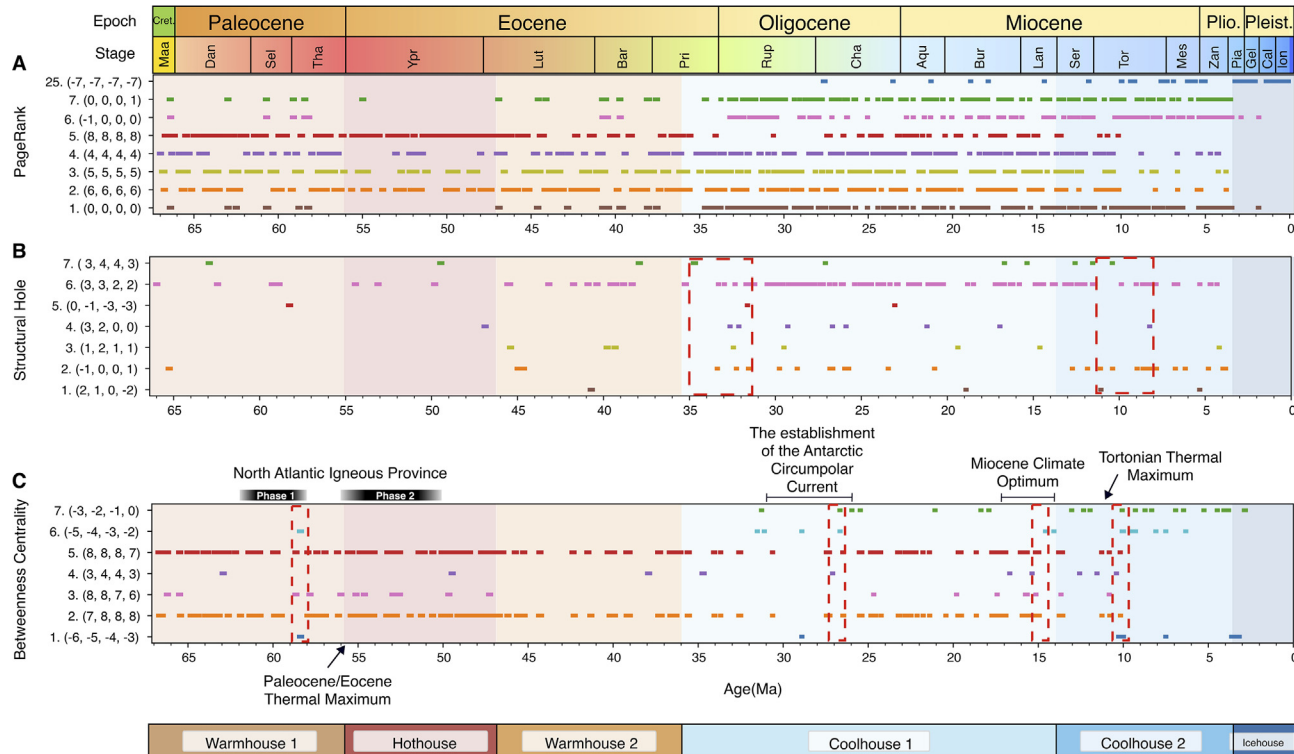


Fig. 16. Spectral plot of control points over time. In (A) and (C) the nodes are sorted in descending order, and in (B) in ascending order. In (A) pattern 25 is the first negative correlation node to appear. In (B), the time periods with 5 or more structural hole nodes within 4 million years are marked separately. In (C) the time periods with 5 or more higher betweenness centrality nodes within 1 million year are marked separately. Abbreviations used in the figure are explained in Fig. 5.

Writing – review & editing, Funding acquisition. **Yongjian Huang**: Writing – review & editing, Data curation, Funding acquisition.

Declaration of Competing Interest

The authors declare that they have no known competing financial interests or personal relationships that could have appeared to influence the work reported in this paper.

Acknowledgements

The authors are very grateful to Prof. M. Santosh, Dr. Yirang Jang and other anonymous reviewers for their constructive and substantive comments on our paper, which have considerably improved its presentation and quality. This work is supported by 2022 Subject Development Research Fund Project of China University of Geosciences, Beijing (Grant No. 2022XK211) and 2023 Graduate Innovation Fund Project of China University of Geosciences, Beijing (Grant No. YB2023YC014). This research is also supported by the National Natural Science Foundation of China (Grant No. 42174149 and No. 42272134).

Appendix A. Supplementary data

Supplementary data associated with this article can be found, in the online version, at <https://doi.org/10.1016/j.gsf.2024.101805>.

References

- Bailey, I., Hole, G.M., Foster, G.L., Wilson, P.A., Storey, C.D., Trueman, C.N., Raymo, M.E., 2013. An alternative suggestion for the Pliocene onset of major northern hemisphere glaciation based on the geochemical provenance of North Atlantic Ocean ice rafted debris. *Quat. Sci. Rev.* 75, 181–194. <https://doi.org/10.1016/j.quascirev.2013.06.004>.
- Basak, C., Martin, E.E., 2013. Antarctic weathering and carbonate compensation at the Eocene-Oligocene transition. *Nat. Geosci.* 6, 121–124. <https://doi.org/10.1038/ngeo1707>.
- Bickel, P.J., Chen, A., 2009. A nonparametric view of network models and Newman-Girvan and other modularities. *Proc. Natl. Acad. Sci. U.S.A.* 106, 21068–21073. <https://doi.org/10.1073/pnas.0907096106>.
- Boers, N., Kurths, J., Marwan, N., 2021. Complex systems approaches for Earth system data analysis. *J. Phys.-Complex.* 2, 011001. <https://doi.org/10.1088/2632-072X/abd8db>.
- Bouttes, N., Roche, D.M., Paillard, D., 2012. Systematic study of the impact of fresh water fluxes on the glacial carbon cycle. *Clim. Past.* 8, 589–607. <https://doi.org/10.5194/cp-8-589-2012>.
- Brandes, U., 2001. A faster algorithm for betweenness centrality. *J. Math. Sociol.* 25, 163–177. <https://doi.org/10.1080/0022250X.2001.9990249>.
- Bridges, J.D., Tarduno, J.A., Cottrell, R.D., Herbert, T.D., 2023. Rapid strengthening of westerlies accompanied intensification of Northern Hemisphere glaciation. *Nat. Commun.* 14, 3905. <https://doi.org/10.1038/s41467-023-39557-4>.
- Cao, W., Xi, D., Melinte-Dobrescu, M.C., Jiang, T., Wise, S.W., Wan, X., 2018. Calcareous nannofossil changes linked to climate deterioration during the Paleocene-Eocene thermal maximum in Tarim Basin, NW China. *Geosci. Front.* 9, 1465–1478. <https://doi.org/10.1016/j.gsf.2018.04.002>.
- Cauvy-Fraunié, S., Condom, T., Rabatel, A., Villacis, M., Jacobsen, D., Dangles, O., 2013. Technical note: glacial influence in tropical mountain hydrosystems evidenced by the diurnal cycle in water levels. *Hydrol. Earth Syst. Sci.* 17, 4803–4816. <https://doi.org/10.5194/hess-17-4803-2013>.
- Cornual, P., Westerhold, T., Pälike, H., Bickert, T., Baumann, K.H., Kucera, M., 2023. Nature and origin of variations in pelagic carbonate production in the tropical ocean since the mid-Miocene (ODP Site 927). *Biogeosciences* 20, 597–618. <https://doi.org/10.5194/bg-20-597-2023>.
- Cotton, L.J., Pearson, P.N., 2011. Extinction of larger benthic foraminifera at the Eocene/Oligocene boundary. *Paleogeogr. Paleoclimatol. Paleoccol.* 311, 281–296. <https://doi.org/10.1016/j.palaeo.2011.09.008>.
- Coxall, H.K., Wilson, P.A., Pälike, H., Lear, C.H., Backman, J., 2005. Rapid stepwise onset of Antarctic glaciation and deeper calcite compensation in the Pacific Ocean. *Nature* 433, 53–57. <https://doi.org/10.1038/nature03135>.
- De Vleeschouwer, D., Drury, A.J., Vahlenkamp, M., Rochholz, F., Liebrand, D., Pälike, H., 2020. High-latitude biomes and rock weathering mediate climate–carbon cycle feedbacks on eccentricity timescales. *Nat. Commun.* 11, 5013. <https://doi.org/10.1038/s41467-020-18733-w>.
- Fasano, G., Franceschini, A., 1987. A multidimensional version of the Kolmogorov-Smirnov test. *Mon. Not. Roy. Astron. Soc.* 225, 155–170. <https://doi.org/10.1093/mnras/225.1.155>.
- Gallegati, M., 2018. A systematic wavelet-based exploratory analysis of climatic variables. *Clim. Change* 148, 325–338. <https://doi.org/10.1007/s10584-018-2172-8>.
- Gasson, E.G.W., DeConto, R.M., Pollard, D., Clark, C.D., 2018. Numerical simulations of a kilometre-thick Arctic ice shelf consistent with ice grounding observations. *Nat. Commun.* 9, 1510. <https://doi.org/10.1038/s41467-018-03707-w>.
- Gleich, D.F., 2015. PageRank beyond the Web. *SIAM Rev.* 57, 321–363. <https://doi.org/10.1137/140976649>.
- Harzhauser, M., Peresson, M., Benold, C., Mandic, O., Čorić, S., Lange, G.J.D., 2023. Environmental shifts in and around Lake Pannon during the Tortonian Thermal Maximum based on a multi-proxy record from the Vienna Basin (Austria, Late Miocene, Tortonian). *Paleogeogr. Paleoclimatol. Paleoccol.* 610, 111332. <https://doi.org/10.1016/j.palaeo.2022.111332>.
- Hill, D.J., Haywood, A.M., Valdes, P.J., Francis, J.E., Lunt, D.J., Wade, B.S., Bowman, V.C., 2013. Paleogeographic controls on the onset of the Antarctic circumpolar current. *Geophys. Res. Lett.* 40, 5199–5204. <https://doi.org/10.1002/grl.50941>.
- Hu, P., Mei, T., 2018. Ranking influential nodes in complex networks with structural holes. *Physica A* 490, 624–631. <https://doi.org/10.1016/j.physa.2017.08.049>.
- Jolivet, M., Boulvais, P., 2021. Global significance of oxygen and carbon isotope compositions of pedogenic carbonates since the Cretaceous. *Geosci. Front.* 12, 101132. <https://doi.org/10.1016/j.gsf.2020.12.012>.
- Jones, S.M., Hoggett, M., Greene, S.E., Dunkley Jones, T., 2019. Large Igneous Province thermogenic greenhouse gas flux could have initiated Paleocene-Eocene Thermal Maximum climate change. *Nat. Commun.* 10, 5547. <https://doi.org/10.1038/s41467-019-12957-1>.
- Lindsay, J.J., Hughes, H.S.R., Yeomans, C.M., Andersen, J.C.Ø., McDonald, I., 2021. A machine learning approach for regional geochemical data: platinum-group element geochemistry vs geodynamic settings of the North Atlantic Igneous Province. *Geosci. Front.* 12, 101098. <https://doi.org/10.1016/j.gsf.2020.10.005>.
- Longman, J., Mills, B.J.W., Donnadieu, Y., Goddérus, Y., 2022. Assessing volcanic controls on Miocene climate change. *Geophys. Res. Lett.* 49, e2021GL096519. <https://doi.org/10.1029/2021GL096519>.
- Ma, X., Ma, W., Tian, J., Yu, J., Huang, E., 2022. Ice sheet and terrestrial input impacts on the 100-kyr ocean carbon cycle during the Middle Miocene. *Glob. Planet. Change* 208, 103723. <https://doi.org/10.1016/j.gloplacha.2021.103723>.
- Marwan, N., Carmen Romano, M., Thiel, M., Kurths, J., 2007. Recurrence plots for the analysis of complex systems. *Phys. Rep.-Rev. Sec. Phys. Lett.* 438, 237–329. <https://doi.org/10.1016/j.physrep.2006.11.001>.
- Morita, K., 2023. A fine-grained distinction of coarse graining. *Eur. J. Philos. Sci.* 13, 12. <https://doi.org/10.1007/s13194-023-00513-0>.
- Myers, A.D., Chumley, M.M., Khasawneh, F.A., Munch, E., 2023. Persistent homology of coarse-grained state-space networks. *Phys. Rev. E* 107, 034303. <https://doi.org/10.1103/PhysRevE.107.034303>.
- Nowack, P., Runge, J., Eyring, V., Haigh, J.D., 2020. Causal networks for climate model evaluation and constrained projections. *Nat. Commun.* 11, 1415. <https://doi.org/10.1038/s41467-020-15195-y>.
- Okuno, J., Miura, H., 2013. Last deglacial relative sea level variations in Antarctica derived from glacial isostatic adjustment modelling. *Geosci. Front.* 4, 623–632. <https://doi.org/10.1016/j.gsf.2012.11.004>.
- Rohling, E.J., Hibbert, F.D., Williams, F.H., Grant, K.M., Marino, G., Foster, G.L., Hennekam, R., Lange, G.J.D., Roberts, A.P., Yu, J., Webster, J.M., Yokoyama, Y., 2017. Differences between the last two glacial maxima and implications for ice-sheet, $\delta^{18}\text{O}$, and sea-level reconstructions. *Quat. Sci. Rev.* 176, 1–28. doi: 10.1016/j.quascirev.2017.09.009.
- Runge, J., Bathiany, S., Bollt, E., Camps-Valls, G., Coumou, D., Deyle, E., Glymour, C., Kretschmer, M., Mahecha, M.D., Muñoz-Marí, J., Van Nes, E.H., Peters, J., Quax, R., Reichstein, M., Scheffer, M., Schölkopf, B., Spirtes, P., Sugihara, G., Sun, J., Zhang, K., Zscheischler, J., 2019. Inferring causation from time series in Earth system sciences. *Nat. Commun.* 10, 2553. <https://doi.org/10.1038/s41467-019-10105-3>.
- Runge, J., Nowack, P., Kretschmer, M., Flaxman, S., Sejdinovic, D., 2019. Detecting and quantifying causal associations in large nonlinear time series datasets. *Sci. Adv.* 5, 4996. <https://doi.org/10.1126/sciadv.aau4996>.
- Saramaki, J., Kivelä, M., Onnela, J.P., Kaski, K., Kertesz, J., 2007. Generalizations of the clustering coefficient to weighted complex networks. *Phys. Rev. E* 75, 027105. <https://doi.org/10.1103/PhysRevE.75.027105>.
- Spray, J.F., Bohaty, S.M., Davies, A., Bailey, I., Romans, B.W., Cooper, M.J., Milton, J.A., Wilson, P.A., 2019. North Atlantic evidence for a unipolar icehouse climate state at the Eocene-Oligocene transition. *Paleoceanogr. Paleoclimatol.* 34, 1124–1138. <https://doi.org/10.1029/2019PA003563>.
- Takemoto, K., Oosawa, C., Akutsu, T., 2007. Structure of n-clique networks embedded in a complex network. *Physica A* 380, 665–672. <https://doi.org/10.1016/j.physa.2007.02.042>.
- Thomas, D.J., Bralower, T.J., 2005. Sedimentary trace element constraints on the role of North Atlantic Igneous Province volcanism in late Paleocene-early Eocene environmental change. *Mar. Geol.* 217, 233–254. <https://doi.org/10.1016/j.margeo.2005.02.009>.
- Tomás, R., Li, Z., Lopez-Sánchez, J.M., Liu, P., Singleton, A., 2016. Using wavelet tools to analyse seasonal variations from InSAR time-series data: a case study of the Huangtupo landslide. *Landslides* 13, 437–450. <https://doi.org/10.1007/s10346-015-0589-y>.

- Turner, S.K., 2014. Pliocene switch in orbital-scale carbon cycle/climate dynamics: Pliocene carbon cycle switch. *Paleoceanography* 29, 1256–1266. <https://doi.org/10.1002/2014PA002651>.
- Wang, M., Tian, L., 2016. From time series to complex networks: the phase space coarse graining. *Physica A* 461, 456–468. <https://doi.org/10.1016/j.physa.2016.06.028>.
- Weng, H., Maleki, A., Zheng, L., 2018. Overcoming the limitations of phase transition by higher order analysis of regularization techniques. *Ann. Stat.* 46, 3099–3129. <https://doi.org/10.1214/17-AOS1651>.
- Westerhold, T., Marwan, N., Drury, A.J., Liebrand, D., Agnini, C., Anagnostou, E., Barnet, J.S.K., Bohaty, S.M., De Vleeschouwer, D., Florindo, F., Frederichs, T., Hodell, D.A., Holbourn, A.E., Kroon, D., Lauretano, V., Littler, K., Lourens, L.J., Lyle, M., Pälike, H., Röhl, U., Tian, J., Wilkens, R.H., Wilson, P.A., Zachos, J.C., 2020. An astronomically dated record of Earth's climate and its predictability over the last 66 million years. *Science* 369, 1383–1387. <https://doi.org/10.1126/science.aba6853>.
- Xiang, Y., Ding, J., Tarokh, V., 2018. Evolutionary spectra based on the multitaper method with application to stationarity test. In: 2018 IEEE International Conference on Acoustics, Speech and Signal Processing (ICASSP), Calgary, AB, pp. 3994–3998. <https://doi.org/10.1109/ICASSP.2018.8461443>.
- Zhang, C., Guo, Z., 2014. Clay mineral changes across the Eocene-Oligocene transition in the sedimentary sequence at Xining occurred prior to global cooling. *Paleogeogr. Paleoclimatol. Paleoecol.* 411, 18–29. <https://doi.org/10.1016/j.palaeo.2014.06.031>.
- Zhang, J., Zhou, J., Tang, M., Guo, H., Small, M., Zou, Y., 2017. Constructing ordinal partition transition networks from multivariate time series. *Sci. Rep.* 7, 7795. <https://doi.org/10.1038/s41598-017-08245-x>.
- Zou, Y., Donner, R.V., Marwan, N., Donges, J.F., Kurths, J., 2019. Complex network approaches to nonlinear time series analysis. *Phys. Rep.-Rev. Sec. Phys. Lett.* 787, 1–97. <https://doi.org/10.1016/j.physrep.2018.10.005>.